
FunctionEvolve: Structure-Guided Symbolic Regression with LLMs

Zeyu Xia^{1,2} Jun Zhu^{2,3} Dong Yan^{1*}

¹Bosch Center for Artificial Intelligence

²Department of Computer Science and Technology, Tsinghua University

³Tsinghua-Bosch Joint Center for ML, Tsinghua University

xia-zy25@mails.tsinghua.edu.cn

dcszj@mail.tsinghua.edu.cn

sproblvem@gmail.com

Abstract

Symbolic regression aims to uncover explicit scientific laws from data. Recent methods use LLMs to guide mutation from background text, which is more directed than random genetic programming. However, exact symbolic recovery requires both semantic guidance and explicit structure, so that domain-informed search are carried out through valid symbolic representation. Current LLM-driven systems remain structure-blind: they select among opaque candidates, lack explicit mechanisms for local mutation, and rely on brittle coefficient fitting that can under-value correct skeletons. We propose FunctionEvolve, an evolutionary framework using expression trees to organize the whole search: structural summaries promote diverse parent selection, local tree edits preserve useful subexpressions, and structure-aware fitting decomposes, constrains, and simplifies coefficients for more reliable scoring. It uses only elementary function families, without additional domain-specific rules limiting generalization. On the 129-task synthetic subset of LLM-SRBench, FunctionEvolve with *Claude Opus 4.6* recovers 107 exact forms, reaching 82.9% SA@50, 4.5x above same-backbone baselines, and 55.8% SA@1, 3.6x above the strongest previously published top-1 result. Ablations show that structure-visible search is central to reliable recovery, with LLM-guided refinements and structure-aware coefficient optimization serving as essential proposal and scoring mechanisms. We also audit the benchmark and show that collinearity in its materials-science subset creates identifiability issues.

1 Introduction

Scientific discovery increasingly requires methods that infer interpretable laws from experimental data [Kramer et al., 2023]. Black-box models can fit observations well, but they often obscure the mechanisms governing natural phenomena. Symbolic Regression (SR) addresses this gap by recovering explicit mathematical expressions from data [Langley, 1981], enabling interpretation, extrapolation, and knowledge transfer [Schmidt and Lipson, 2009].

SR searches a combinatorial space of formulas, and genetic programming (GP) remains a standard way to represent expressions as abstract syntax trees (ASTs) and evolve them through local operators [Koza, 1994]. However, SR is NP-hard [Virgolin and Pissis, 2022], and GP driven mainly by random variation and data-fit selection often lacks the scientific priors needed to navigate large hypothesis spaces efficiently. Recent LLM-driven methods therefore use background information typically describes the data scenario, including variable meanings and the scientific process being modeled

*Corresponding author.

and model knowledge to guide equation discovery. However, new synthetic benchmarks show that semantic guidance alone still leaves a large gap in exact symbolic recovery [Shojaee et al., 2025].

This gap prompts a necessary re-examination of current SR methodologies. We identify three shared bottlenecks in traditional GP and its LLM-driven variants. First, the search often starts from generic seeds rather than useful structural priors. Second, parent selection is usually driven by fixed heuristics over opaque candidates, making it difficult to allocate search budget across genuinely different skeletons. Third, unreliable coefficient optimization can make structurally correct skeletons appear unpromising, causing them to be discarded prematurely.

Explicit expression structure offers a direct way to address these bottlenecks, especially for mutation, where progress often comes from local edits rather than full rewrites. For example, if the current candidate is $a_1 \sin(x) + a_2x$ and the target is $b_1 \sin(b_2x + b_3) + b_4x^{b_5}$, the remaining progress mainly requires editing the sine argument and the power term while preserving the rest. This is precisely where structure matters. GP can modify subexpressions without rewriting the whole formula, but its edits are largely random and do not exploit task context. Prior LLM-driven systems are more directed, but their textual or code-level edits are not necessarily AST-local, so semantically plausible revisions can still overwrite useful parent structure. FunctionEvolve therefore makes AST structure explicit and operative: AST-rule edits provide systematic local add/delete operations, while LLM-guided proposals use the exposed tree structure to make context-dependent refinements that preserve useful parent substructures. Beyond mutation, the same explicit AST structure helps the Selector enforce structural diversity and gives the structure-aware coefficient optimizer the skeleton needed to separate linear from nonlinear parameters, snap structurally constrained exponents, and simplify algebraically equivalent forms, reducing coefficient-search difficulty.

Core insight: Explicit AST structure makes mutation follow SR’s local-editing nature and also benefits parent-diversity selection and coefficient fitting.

Building on this insight, we develop FunctionEvolve as an equation-discovery framework organized around AST-visible search. Our contributions are as follows:

- We present FunctionEvolve, a structure-guided LLM framework for equation discovery that uses explicit expression trees to coordinate selection, mutation, and coefficient optimization.
- On the 129-task synthetic subset of LLM-SRBench, FunctionEvolve achieves 82.9% SA@50 and 55.8% SA@1 with *Claude Opus 4.6*, corresponding to a 4.5x improvement over same-backbone baselines and a 3.6x top-1 improvement over strongest published PiT-PO.
- Ablations show that structure-visible search, LLM-guided local refinements, and structure-aware coefficient optimization are all critical for reliable symbolic recovery.
- We identify critical limitations in LLM-SRBench, including input-variable linear dependence and weak nonlinear factor variation that undermine structural identifiability.

2 Related Work

Symbolic regression has long been studied as a route to scientific discovery, from early empirical-law discovery systems [Langley, 1981] to later work recovering interpretable laws from experimental data [Schmidt and Lipson, 2009]. Modern SR spans symbolic neural networks, reinforcement learning, physics-inspired methods, and evolutionary systems [Martius and Lampert, 2016, Sahoo et al., 2018, Petersen et al., 2021, Udrescu and Tegmark, 2020, Cranmer, 2023]. Among them, GP-style methods remain strong baselines in comparisons [Cava et al., 2021]: they represent expressions as trees [Koza, 1994], enabling structured variation operators such as context-preserving, grammar-based, and strongly typed GP [D’haeseleer, 1994, Whigham, 1995, Montana, 1995]. Related work on prior-guided seeding, diversity, and coefficient fitting shows that symbolic recovery benefits from both expression-structure search and reliable numerical parameter identification [Lu et al., 2015, Mundhenk et al., 2021, Burlacu et al., 2023, Kommenda et al., 2020, dos Reis et al., 2024].

Recent work applies LLMs to SR by using model knowledge and task context to guide equation proposal, refinement, or selection. Representative systems include LLM-SR, LLM4Ed, DRSR, SR-Scientist, PiT-PO, and LaSR [Shojaee et al., 2024, Du et al., 2024, Wang et al., 2025, Xia et al., 2025, Wang et al., 2026, Grayeli et al., 2024]; evolutionary coding agents such as OpenEvolve, AlphaEvolve, and ShinkaEvolve also demonstrate LLM-guided program evolution [Sharma, 2025,

Novikov et al., 2025, Lange et al., 2025]. These methods add semantic guidance beyond random GP, but often treat expressions as strings, programs, or opaque candidates rather than explicit expression trees shared across selection, mutation, and fitting.

The rise of LLM-based SR also makes benchmark design more important. Literature-derived benchmarks such as AI-Feynman, SRBench, and EmpiricalBench are valuable but may overlap with LLM pretraining data [Udrescu and Tegmark, 2020, Cava et al., 2021, Cranmer, 2023]. LLM-SRBench reduces this risk with synthetic scientific tasks and shows that existing LLM-driven SR methods still struggle with exact symbolic recovery [Shojaee et al., 2025]; FunctionEvolve targets this gap with AST-visible LLM search and structure-aware coefficient fitting.

3 Method

3.1 Problem Formulation

We consider LLM-driven symbolic regression over a dataset $\mathcal{D} = \{(\mathbf{x}_i, y_i)\}_{i=1}^n$ together with a task-level context T , where $\mathbf{x}_i \in \mathbb{R}^d$ is the numerical input and $y_i \in \mathbb{R}$ is the target. The context T is a natural-language description of the task that is shared across all n samples; depending on the benchmark, it may include the problem background and scientific scenario, the data source, and the names, physical meanings, and units (dimensions) of the variables. For dimension-only tasks such as AI-Feynman entries, T may provide only variable names and units. The goal is to recover a concise, generalizable expression \tilde{f} with $\tilde{f}(\mathbf{x}_i) \approx y_i$, using T to guide the search.

3.2 Overview

Our method formulates SR as one-shot initialization followed by iterative evolution. FunctionEvolve first uses the Generator to synthesize task-conditioned domain knowledge and seed expressions. It then uses the Selector to choose promising parents, the Mutator to expand them through AST-rule and LLM-guided mutations, and the structure-aware Optimizer to fit, simplify, and score valid offspring before reinsertion. Unlike prior LLM-driven methods, FunctionEvolve uses LLMs for seed generation, parent selection, and mutation, with each part anchored to explicit expression structure. The workflow is illustrated in Figure 1, and the complete algorithm is in Appendix C1.

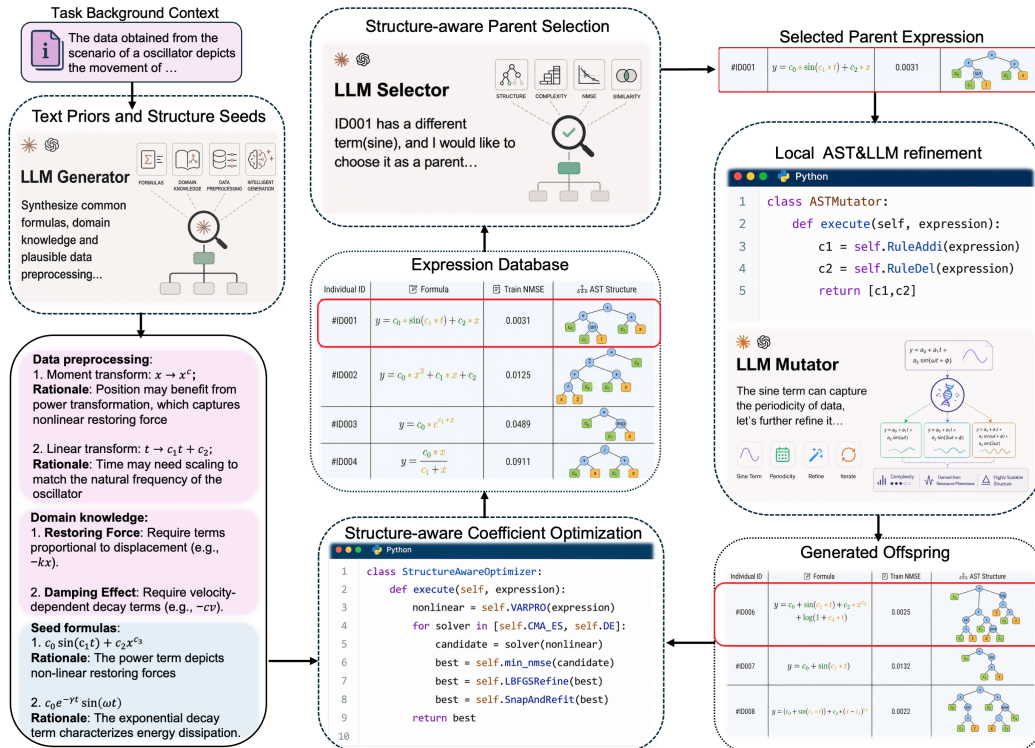


Figure 1: FunctionEvolve initializes candidate expressions from task context and then iteratively selects, mutates, optimizes, and evaluates them over an evolving expression database.

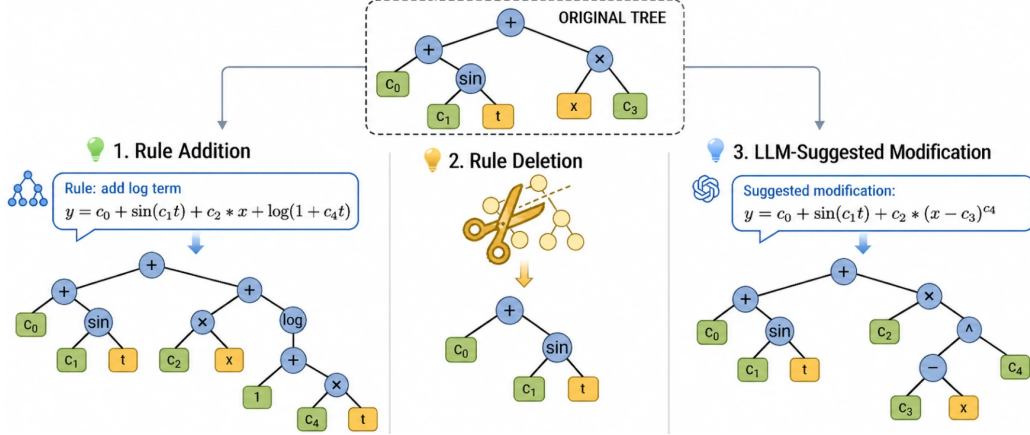


Figure 2: AST rule add/del and LLM-guided local mutation generate offspring from selected parents.

3.3 Generator

The Generator provides task-conditioned structural starting points through two roles: (1) it uses the available task context and LLM knowledge to synthesize domain formulas and structural heuristics; and (2) it initializes seed expressions from these patterns so the search does not begin from an unstructured pool. These outputs provide initial starting points and reusable contextual guidance for evolution, rather than encoded domain laws or fixed mutation rules. Details of the Generator procedure and prompt are provided in Appendix C2.

3.4 Selector

The Selector determines which expressions to expand next. Each iteration, the system extracts an evolution-tree summary and provides it to the Selector with the task context and previous selections. For each candidate node, this summary combines structural information (AST structure, parameter count, tree depth, and operator counts) with numerical information (training NMSE and fitted parameter values). Based on this information, the Selector returns a small set of parent nodes, allocating limited search budget to more promising directions. Details of the evolutionary tree and Selector are provided in Appendices C3 and C4, respectively.

The Selector is not purely greedy: it favors low-error, simple candidates while using selection history to avoid repeatedly expanding similar branches. To prevent data leakage, the tree summary exposes only training error, never test or out-of-distribution error.

3.5 Mutator

The Mutator generates candidates by locally adjusting parent nodes selected by the Selector. For each selected parent expression $f(\mathbf{x}; \mathbf{c})$, it applies three complementary operations, as illustrated in Figure 2: (1) *Rule addition*, which preserves the parent and attaches fixed elementary functions (Table 1) through a small set of attachment operators detailed below; (2) *Rule deletion*, which prunes or unwraps AST substructures to test whether current formula parts are redundant; and (3) *LLM-guided proposal*, which uses parent structure, fitted information, rule-generated candidates, search history, and domain knowledge to suggest non-template, context-dependent refinements.

Table 1: Elementary content library used by rule-addition. For multivariate tasks, single-variable templates instantiate for each x_j , while pair families use ordered variable pairs (x_i, x_j) .

Family	Library content g	Multivariate handling
Linear	$c_1 x_j + c_2$	—
Trigonometric	$c_1 \sin(c_2 x_j + c_3)$	—
Power	$c_1 x_j^{c_2}$	$c_1 (x_i + c_2)^{c_3} x_j$
Exponential	$c_1 \exp(c_2 x_j)$	—
Logarithmic	$c_1 \log(1 + c_2 x_j)$	—
Rational-fraction	$(c_1 x_j + c_2) / (c_3 x_j + c_4)$	$(c_1 x_i + c_2) / (c_3 x_j + c_4)$

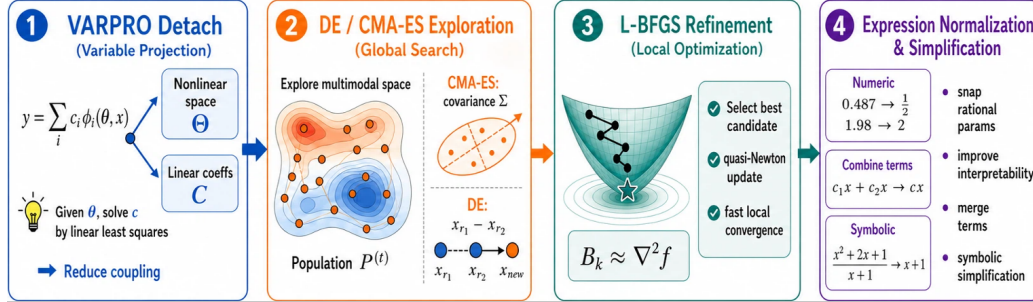


Figure 3: Structure-aware optimizer pipeline: variable projection, DE/CMA-ES global exploration, L-BFGS local refinement, parameter snapping, and symbolic simplification.

The deterministic library uses only generic elementary content and common algebraic attachment operators, without domain-specific rules. Rule addition combines this content with the parent through addition, multiplication, and division; unary wraps additionally apply $\exp(cf)$, $\log(1 + cf)$, $\sin(cf)$, $|cf|$, and f^c . Its breadth comes from operator families rather than benchmark- or domain-level priors, preserving low inductive bias while making compact products, ratios, and compositions reachable. After mutation, candidates are normalized and deduplicated by structural fingerprints before entering the expression database. This design combines reliable rule-based local search with flexible LLM-guided refinements, allowing the search to expand beyond fixed templates while avoiding saturation by repeated or invalid candidates. Details of the AST representation, rule-based and LLM-guided mutation, and normalization procedures are provided in Appendix C5.

3.6 Optimizer

The Optimizer fits coefficients for each fixed candidate skeleton and returns its score. Rather than treating coefficient fitting as black-box optimization, FunctionEvolve exploits expression structure throughout the pipeline (Figure 3). Coefficients at different structural positions carry algebraic priors: linear parameters can be solved by variable projection and OLS, remaining nonlinear parameters are searched with global and local optimizers, structurally constrained parameters can be snapped to stable integer or rational values, and redundant forms can be removed through coefficient merging and symbolic simplification before refitting. These priors reduce redundant dimensionality and make correct skeletons less likely to be discarded because of poor exploration or local optima. They are generic SR operations and therefore do not encode benchmark shortcuts. See Appendix C6 for details.

4 Experiments

4.1 Main Results

The main comparison in this subsection is conducted on the synthetic benchmark set of LLM-SRBench [Shojaee et al., 2025]. We choose this benchmark because its synthetic construction reduces the risk of contamination from memorized formulas in LLM pretraining, thereby providing a cleaner test bed for the primary symbolic-regression comparison.

Symbolic regression is commonly evaluated using three complementary metrics: (1) **Symbolic accuracy at k** ($SA@k$), whether at least one of the top- k candidates ranked by training NMSE matches the ground-truth symbolic structure, usually evaluated using an LLM-as-a-judge protocol; (2) **Accuracy to tolerance** Acc_τ , the number of tasks whose top-1 candidate reaches maximum relative error over all evaluation points at most τ , where τ is typically set to 0.1 or 0.01; and (3) **Normalized mean squared error (NMSE)**, a metric that measures aggregate numerical error.

Since $SA@k$ is calculated based on LLMs, we further audit the reliability of its LLM-as-a-judge protocol. On 500 sampled verification cases, *GPT-5.2* and *Claude Opus 4.6* agree on 476 decisions; manual auditing over these 500 cases gives judge accuracies of 96.4% and 98.6%, respectively. In the actual experiments, each candidate is verified by both models: agreeing verdicts are accepted, while disagreements are manually adjudicated (See Appendix D6).

Table 2 reports symbolic accuracy and numerical accuracy for each domain and for the full 129-task benchmark. We emphasize both $SA@50$ and $SA@1$: $SA@50$ measures whether the search generates a correct symbolic form within its top-50 training-NMSE-ranked candidates, while $SA@1$ measures whether the method’s single selected expression already recovers the target structure. Numerical

Table 2: Main results on the 129-task synthetic subset of LLM-SRBench. Entries report SA@50 (SA@1), Acc_{0.1} task counts, and median test NMSE; table headers abbreviate these as SA, Acc, and NMSE. Parenthesized-only SA values are published top-1 results without reported SA@50. Bold marks the best non-reference values, while the ground-truth row is a reference upper bound. * and ** denote results cited from LLM-SRBench [Shojaee et al., 2025] and PiT-PO [Wang et al., 2026].

Model	Chemistry (36)			Biology (24)			Physics (44)			MatSci (25)			Total (129)		
	SA↑	Acc↑	NMSE↓	SA↑	Acc↑	NMSE↓	SA↑	Acc↑	NMSE↓	SA↑	Acc↑	NMSE↓	SA↑	Acc↑	NMSE↓
<i>Direct Prompting</i>															
<i>GPT-4o-mini</i> [*]	(0)	5	0.0221	(0)	1	0.4648	(2)	4	0.0647	(0)	0	0.0484	(2)	10	–
<i>Claude Opus 4.6</i>	0 (0)	3	1.50e-2	1 (1)	3	2.43e-4	0 (0)	4	2.18e-3	1 (0)	8	2.86e-5	2 (1)	18	1.36e-3
<i>PySR [Cranmer, 2023]</i>															
PySR [*]	(0)	15	–	(0)	6	–	(2)	13	–	(0)	17	–	(2)	51	–
<i>OpenEvolve [Sharma, 2025]</i>															
<i>Claude Opus 4.6</i>	7 (2)	11	8.19e-7	8 (1)	2	9.37e-6	0 (0)	5	1.21e-4	9 (2)	9	1.07e-7	24 (5)	27	4.30e-6
<i>LaSR [Grayeli et al., 2024]</i>															
Llama-3.1-8B [*]	(0)	10	2.77e-4	(1)	4	2.73e-4	(2)	11	0.0018	(2)	16	7.44e-5	(5)	41	–
<i>GPT-4o-mini</i> [*]	(1)	14	9.11e-5	(2)	5	1.53e-4	(4)	14	9.94e-4	(7)	18	9.23e-6	(14)	51	–
<i>LLM-SR [Shojaee et al., 2024]</i>															
<i>GPT-4o-mini</i> [*]	(4)	19	4.12e-6	(4)	7	3.06e-6	(4)	16	7.62e-5	(5)	22	3.21e-9	(17)	64	–
<i>Claude Opus 4.6</i> ³	9 (4)	14	4.13e-7	8 (5)	6	2.15e-7	0 (0)	3	7.11e-5	7 (2)	17	2.90e-9	24 (11)	40	9.80e-7
<i>PiT-PO [Wang et al., 2026]</i>															
Llama-3.1-8B (RL) ^{**}	(5)	28	4.13e-7	(7)	17	9.37e-8	(5)	18	6.57e-5	(3)	23	1.18e-8	(20)	86	–
<i>FunctionEvolve (Ours)</i>															
No LLM	7 (3)	32	1.76e-12	12 (8)	16	6.66e-13	7 (5)	11	1.89e-5	3 (0)	19	2.83e-14	29 (16)	78	1.47e-10
Llama-3.1-8B	20 (5)	32	7.52e-13	20 (9)	20	3.85e-13	17 (6)	18	4.59e-8	5 (3)	20	1.20e-14	62 (23)	90	1.17e-12
<i>Qwen3.6-27B</i>	27 (8)	35	1.99e-13	21 (11)	23	2.08e-13	29 (16)	30	5.19e-13	9 (3)	21	1.44e-14	86 (38)	109	2.06e-13
<i>DeepSeek-V4-Pro</i>	32 (21)	34	2.18e-13	20 (14)	23	2.08e-13	33 (30)	33	5.15e-13	14 (6)	21	1.20e-14	99 (71)	111	1.78e-13
<i>GPT-5.2 medium</i>	30 (13)	34	2.08e-13	20 (15)	23	3.80e-13	37 (36)	33	4.03e-13	16 (5)	21	1.32e-14	103 (69)	111	2.08e-13
<i>Claude Opus 4.6</i>	31 (16)	35	1.85e-13	22 (16)	23	2.06e-13	39 (34)	33	2.44e-13	15 (6)	22	1.44e-14	107 (72)	113	1.38e-13
<i>Reference: GT</i>	36 (36)	35	1.49e-13	24 (24)	23	1.43e-13	44 (44)	37	1.14e-13	25 (25)	25	1.87e-14	129 (129)	120	4.98e-14

metrics are complementary: NMSE can be saturated by structurally incorrect surrogate expressions, and worst-point Acc_τ can be brittle when small y_{true} values amplify relative-error thresholds. The ground-truth row is therefore included only as a dataset reference ceiling, not as a competing method.²

FunctionEvolve greatly improves symbolic recovery under both SA@50 and SA@1. The No LLM variant uses generic seed generation without semantic priors, training-NMSE-ranked selection, programmatic AST mutation, and the same structure-aware optimizer. It already recovers 29 SA@50 forms and 16 SA@1 forms, close to the strongest published PiT-PO top-1 result of 20. This shows that GP-style rule mutation combined with reliable structure-aware fitting is itself a strong symbolic-search baseline. Adding LLM-guided generation, selection, and mutation raises SA@50 to 107 with *Claude Opus 4.6*, while the strongest same-backbone rerun baselines, LLM-SR and OpenEvolve, each reach 24. At top-1, FunctionEvolve reaches 72 SA@1, exceeding PiT-PO by 3.6x.

Additional backbones show the same trend: *DeepSeek-V4-Pro* recovers 99 (71) tasks and is especially strong on chemistry, the mid-sized open-weight *Qwen3.6-27B* reaches 86 (38), and *Llama-3.1-8B* reaches 62 (23), improving substantially over the No LLM setting in SA@50 but only slightly in SA@1. This is notable because PiT-PO also builds on the Llama-3.1-8B backbone but further applies reinforcement learning, whereas our Llama-3.1-8B run uses no RL and still surpasses PiT-PO. In

²An additional baseline, SR-Scientist [Xia et al., 2025], is compared separately in Appendix D5 rather than in this table: its headline Acc_τ discards the worst 5% of evaluation points before taking the maximum, making it a relaxed variant aligned with our 95%Acc_τ rather than our strict all-point Acc_τ, and it reports symbolic accuracy only for a few representative methods, without an SA@k analysis.

³The public LLM-SRBench code reports only top-1 symbolic accuracy. We additionally audit the top-50 training-NMSE-ranked candidates for our *Claude Opus 4.6* rerun and report entries as SA@50 (SA@1). With this released implementation, our rerun is weaker at SA@1 than the originally reported *gpt-4o-mini* result, possibly because the authors used a different evaluation method; related reproducibility concerns are noted by other researchers at <https://openreview.net/forum?id=0L4RWQV8Qa>.

practice, Llama-3.1-8B also has weaker JSON-format following than newer models, so invalid structured outputs are replaced by the deterministic rule-based baseline in our implementation. When the LLM interface fails, the system falls back to the baseline. Therefore, the measured gains provide a conservative estimate of the benefit of LLM-guided search.

The gains are broad across domains: 31/36 chemistry tasks, 22/24 biology tasks, 39/44 physics tasks, and 15/25 materials-science tasks under SA@50, with corresponding SA@1 counts of 16/36, 16/24, 34/44, and 6/25. Worse performance on materials science is partly explained by benchmark identifiability issues discussed in Section 5. The gap between SA@50 and SA@1 shows that correct equations are often generated but not always ranked first by training NMSE. Our inspection suggests this ambiguity arises because some expressions are difficult to distinguish from high-order rational approximations or series expansions, especially over restricted data ranges.

Main result: The main gap for LLM-driven SR lies in symbolic rather than numerical: FunctionEvolve closes much of this gap while preserving near-GT numerical precision.

Numerically, FunctionEvolve with *Claude Opus 4.6* reaches 113 tasks under $Acc_{0.1}$, close to the GT reference value of 120, and maintains median test NMSE at 1.38×10^{-13} . The updated *Llama-3.1-8B* run recovers 62 (23) symbolic forms and has a low median test NMSE of 1.17×10^{-12} , while reaching 90 tasks under $Acc_{0.1}$ and 69/61 tasks under the stricter $Acc_{0.01}/Acc_{0.001}$ thresholds. This gap should not be interpreted as contradicting the symbolic result: exact symbolic recovery is the primary goal of scientific SR, while worst-point Acc_τ is a numerically brittle auxiliary metric on this benchmark. Because Acc_τ divides by y_{true} pointwise, very small y_{true} values can amplify tiny numerical perturbations into threshold failures, so even GT equations may not satisfy the relative-error threshold; Appendix D5 discusses the alternative 95% Acc_τ metric and stricter numerical thresholds. These gains are not due to larger LLM budgets: FunctionEvolve averages 66.86 LLM calls per task, versus 1000.27 for LLM-SR and 201.50 for OpenEvolve, with lower price-weighted token cost than LLM-SR and comparable cost to OpenEvolve (Appendix B).

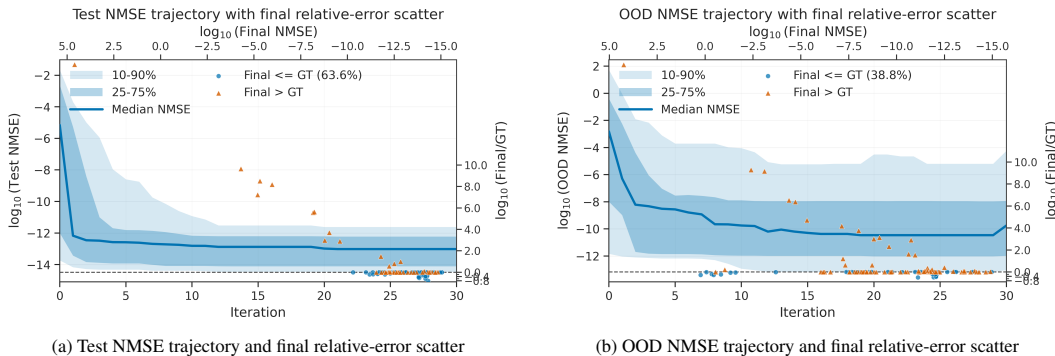


Figure 4: Global NMSE trajectories and final relative errors. Curves show median $\log_{10}(\text{NMSE})$, and shaded bands show 25–75% and 10–90% ranges using bottom and left axes. Overlaid points use top and right axes: horizontal coordinate is $\log_{10}(\text{NMSE}_{\text{final}})$ and vertical coordinate is $\Delta = \log_{10}(\text{NMSE}_{\text{final}}/\text{NMSE}_{\text{GT}})$. Blue circles indicate $\Delta \leq 0$, and orange triangles indicate $\Delta > 0$.

To further inspect the numerical behavior behind the aggregate NMSE values, Figure 4 shows the test and OOD NMSE search trajectories for the strongest *Claude Opus 4.6* setting, with overlaid scatter points comparing final NMSE against the ground-truth NMSE for each task. On the test split, the global-best median NMSE drops to the numerical floor within the first few iterations and then remains close to the ground-truth NMSE distribution, indicating that the optimizer often fits recovered skeletons to near ground-truth numerical precision. This is also reflected in the paired comparison: the final expression is no worse than the ground-truth expression on 82/129 tasks (63.6%).

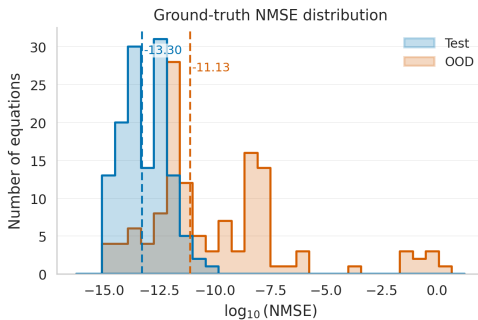


Figure 5: Ground-truth NMSE distributions on the test and OOD splits. OOD has a larger and more dispersed error baseline.

Out-of-distribution evaluation shows the same qualitative error reduction, but the paired comparison is weaker, with 50/129 tasks (38.8%) no worse than ground truth. This gap should be read against Figure 5: even the ground-truth expressions have larger and more dispersed NMSE on held-out OOD samples, with a median about two orders of magnitude higher than on the test split. Thus, this setting has a higher numerical error floor even for the exact laws, and the weaker paired comparison largely reflects the intrinsic difficulty and lower numerical stability of these samples, although task-specific extrapolation effects can still amplify expression-level differences.

4.2 Evaluation on AI-Feynman

We also evaluate FunctionEvolve on the AI-Feynman benchmark family [Udrescu and Tegmark, 2020]. Because recent papers use slightly different protocols, Table 3 reports each result in its native denominator rather than forcing a single leaderboard: LaSR reports the 100 original Feynman equations, SR-LLM reserves 10 of those equations as retrieval knowledge and tests on the remaining 90, and QDSR uses a 117-target Feynman-AI subset. Under the full 120-task setting, consisting of the 100 original equations plus 20 bonus equations, FunctionEvolve recovers all 120 tasks at top-1.

Table 3: Reported exact-recovery results on AI-Feynman-style benchmarks. Protocols differ, so entries keep their original denominators.

Method	Evaluation set	Recovery
LaSR [Grayeli et al., 2024]	100 original	72/100
SR-LLM [Guo et al., 2025]	90 held-out	69/90
QDSR [Bruneton, 2025]	117-target subset	107/117
FunctionEvolve (Ours)	100+20 full set	SA@1 120/120

Figure 6 provides a first-appearance diagnostic for symbolic matches. A match at round 0 means that an equivalent expression was already present in the LLM-proposed seed set, before evolutionary mutation. The AI-Feynman row is much more concentrated at round 0 than the synthetic LLM-SRBench rows, which is consistent with literature-derived equations being easier for the model to recall or directly propose from prior exposure.

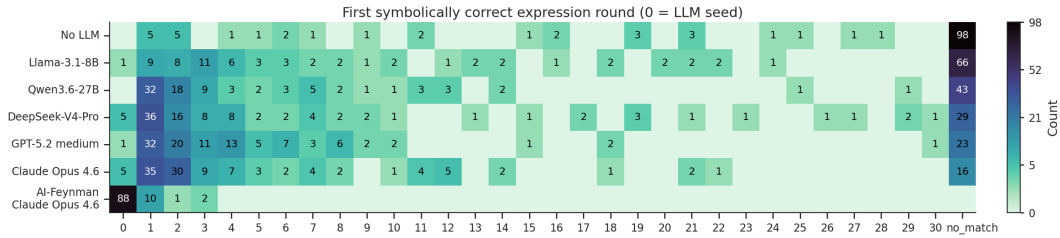


Figure 6: First-appearance round of the first symbolically correct expression for clean runs. Round 0 denotes a correct expression already present in the LLM-proposed seed set, while no_match denotes runs without a symbolic match. The last row shows AI-Feynman results, while the others show LLM-SRBench results; concentration at round 0 evidences stronger AI-Feynman contamination.

These results are complementary to the LLM-SRBench evaluation rather than a replacement for it. AI-Feynman is a standard physics benchmark, but its literature-derived equations may be present in LLM pretraining data; LLM-SRBench therefore remains our primary lower-contamination test bed. The AI-Feynman result mainly shows that the same structure-guided search also performs strongly on the classical physics benchmark, including the harder bonus equations.

4.3 Ablation Study

We further ablate the major components of FunctionEvolve using the degenerated variants described in Appendix C2–C6. The *w/o Generator* setting sets the extracted domain knowledge to empty and initializes the search from a fixed seed list. The *w/o Selector* setting removes the LLM parent-selection module and instead uses Boltzmann sampling over fitness ranks. For mutation, we consider two complementary ablations: *w/o LLM Mutator* disables LLM-generated local structural refinements and keeps only the AST Mutator, while

Table 4: Ablation study on 129 tasks. Entries report total SA@50 (SA@1). Domain-wise SA results are reported in Appendix D4.

Method	GPT-5.2-medium	Claude Opus 4.6
Full	103 (69)	107 (72)
w/o All	35 (6)	34 (10)
w/o Generator	79 (49)	91 (58)
w/o Selector	62 (44)	74 (46)
w/o LLM Mutator	45 (27)	46 (31)
w/o AST Mutator	70 (42)	84 (50)
w/o Struct. Optimizer	46 (16)	53 (22)

w/o AST Mutator disables rule-driven AST additions and deletions and keeps only LLM-generated ADD/SUBST edits. The *w/o Structure-aware Optimizer* setting replaces the structure-aware coefficient optimizer with L-BFGS. Finally, *w/o All* combines *w/o Generator*, *w/o Selector*, *w/o AST Mutator*, and *w/o Structure-aware Optimizer*. In both implementation and experimental behavior, this combined ablation is close to a parallel multi-offspring version of LLM-SR [Shojaee et al., 2024]. Although this parallel setting evaluates more candidate expressions per round, the local evaluations are independent and can be distributed across CPU workers, so wall-clock cost does not increase in proportion to the candidate count; detailed resource comparisons are provided in Appendix B.

Table 4 reports total SA@50 (SA@1) for *GPT-5.2-medium* and *Claude Opus 4.6*; domain-wise breakdowns are provided in Appendix D4. Under *Claude Opus 4.6*, the combined ablation reduces SA from 107 (72) to 34 (10) tasks. Among components, removing the LLM Mutator and the structure-aware optimizer causes the largest SA@50 drops, to 46 (31) and 53 (22), confirming that LLM-guided local refinement and reliable structure-aware coefficient fitting are both essential; removing the AST Mutator and Selector also degrades recovery, to 84 (50) and 74 (46), showing that the strongest performance comes from combining LLM reasoning with explicit symbolic structure and reliable coefficient scoring. We therefore first isolate the contribution of AST visibility, then examine whether candidate skeletons can be scored reliably by the structure-aware coefficient optimizer.

Ablation takeaway: FunctionEvolve succeeds by combining explicit AST structure, reliable structure-aware optimization, and frontier-model symbolic proposals.

4.4 Analysis of AST Structure

To isolate the role of AST structure more directly, we use a stricter *w/o AST Structure* variant under *Claude Opus 4.6*. This variant keeps the LLM Selector and LLM Mutator, but removes all AST-related information and operations: the Selector no longer observes AST-derived structural fields, the AST Mutator is disabled, and the LLM Mutator no longer receives the annotated AST or AST-specific mutation guidance.

As shown in Table 5, removing all AST structure reduces total SA@50 (SA@1) from 107 (72) to 60 (40). This is substantially worse than only removing the AST Mutator, which still obtains 84 (50) when the LLM components can observe AST-derived structure. The gap indicates that AST structure is useful not only as a source

Table 5: Effect of AST structure under *Claude Opus 4.6*. Entries report SA@50 (SA@1).

Variant	Chemistry (36)	Biology (24)	Physics (44)	Materials (25)	Total (129)
Full	31 (16)	22 (16)	39 (34)	15 (6)	107 (72)
w/o AST Mutator	30 (16)	22 (11)	23 (20)	9 (3)	84 (50)
w/o AST Structure	24 (14)	20 (15)	8 (7)	8 (4)	60 (40)

of deterministic rule mutations, but also as an explicit representation that helps the LLM reason about expression complexity, reusable subtrees, and meaningful local edits. The degradation is especially severe on the Physics split, whose equations are more structurally complex in the benchmark.

4.5 Analysis of Structure-aware Coefficient Optimization

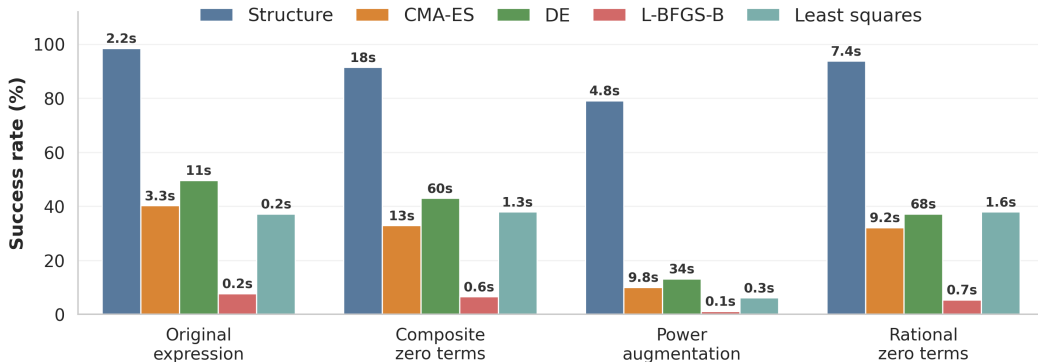


Figure 7: Optimizer benchmark on ground-truth skeletons and transformed variants. Success is defined as $NMSE < 1e-10$; numbers above bars report median runtime.

The ablation in Section 4.3 points to coefficient optimization as a major failure mode: under *Claude Opus 4.6*, replacing the structure-aware coefficient optimizer with L-BFGS-B reduces total SA@50 (SA@1) from 107 (72) to 53 (22). To separate optimizer failure from symbolic-search failure, we benchmark optimizers on ground-truth skeletons and controlled variants (Appendix C7). A run is counted as successful only when the fitted expression reaches $\text{NMSE} < 1e-10$ on the training data. As shown in Figure 7, the structure-aware coefficient optimizer consistently outperforms standalone optimizers across all four transformation groups while keeping median runtime modest. It solves 98.4% of original-expression cases, 91.5% of composite zero-term cases, 79.1% of power-augmentation cases, and 93.8% of rational zero-term cases. This result explains why the optimizer ablation in Table 4 is so large: lacking structural information, a generic optimizer must search a higher-dimensional and less constrained parameter space, making optimization less efficient and more susceptible to local optima. It can therefore underfit otherwise correct symbolic skeletons and create false negatives during fitness evaluation. Consistently, the No LLM row in Table 2 shows pure GP mutation with the structure-aware optimizer already approaches PiT-PO SOTA.

4.6 Analysis under Noisy Observations

We further evaluate FunctionEvolve on noisy versions of LLM-SRBench using the same *Claude Opus 4.6* setting. As shown in Table 6, exact symbolic recovery is sensitive to observation noise: total SA@50 (SA@1) drops from 107 (72) in the clean setting to 54 (24) under 1% noise and 40 (13) under 5% noise. The numerical criterion also degrades sharply, with test $\text{Acc}_{0.1}$ decreasing from 113 tasks to 39 and 23 tasks, respectively. This behavior is expected because the search ranks candidates by noisy training fit while symbolic accuracy is judged against the clean ground-truth expression. Under noise, structurally different expressions can become numerically plausible explanations of the perturbed samples, so the evolutionary search may favor smooth or overfit alternatives that fit the observations but no longer match the exact law. These results suggest that noisy scientific equation discovery requires uncertainty-aware scoring and validation in addition to stronger symbolic search.

4.7 Complexity-aware Final Candidate Selection

The gap between SA@50 and SA@1 indicates that the search often generates a correct expression but does not rank it first by training NMSE. We therefore examine complexity-aware final-candidate selectors for the *Claude Opus 4.6* full run, with the three selection rules summarized in Figure 8. After search terminates, these selectors are applied to the complete expression trajectory to choose the final candidates to report. They are distinct from the evolutionary Selector in Section 3: they do not choose parents, guide mutation, affect coefficient fitting, or otherwise change the search trajectory.

The final-candidate selectors use only training NMSE and expression complexity, never test or OOD NMSE. Pareto performs non-dominated sorting over training NMSE and complexity and fills the reporting budget from successive Pareto layers. The Occam variant first restricts candidates to a near-best training-NMSE neighborhood and then favors simpler expressions using tree size, operator count, parameter count, and special-function count. The MDL variant uses a linear penalty on training loss and complexity features. As shown in Table 7, the five-candidate Pareto and Occam selections recover 102 and 101 exact forms, already above the 95 exact forms obtained by the top-10 training-NMSE ranking and close to the top-50 result of 107. The approximate SA@all value is 113, showing that a few additional exact forms appear deeper in the search trajectory. This suggests that many apparent top-1 failures are final-ranking failures caused by numerically strong but structurally less concise surrogate expressions. However, a gap remains to SA@all, indicating that complexity-aware ranking still cannot always identify the correct form within a very small reporting budget.

Table 6: Robustness under noisy observations with *Claude Opus 4.6*. Entries report counts over 129 tasks.

Setting	SA@50 (SA@1)	$\text{Acc}_{0.1}$	Test NMSE
Clean	107 (72)	113	1.38e-13
1% noise	54 (24)	39	1.32e-6
5% noise	40 (13)	23	3.05e-5

Table 7: Final-candidate selection for the *Claude Opus 4.6* full run on 129 clean LLM-SRBench tasks.

Ranking rule	Shortlist	Exact matches
Train NMSE	1	72
Train NMSE	5	89
Train NMSE	10	95
Pareto	5	102
Occam	5	101
MDL	5	97
Pareto	10	102
Occam	10	104
MDL	10	101
Train NMSE	50	107
Train NMSE	all ⁴	113

⁴Here, “all” denotes SA@all over roughly the top 1000 full-trajectory candidates ranked by training NMSE.

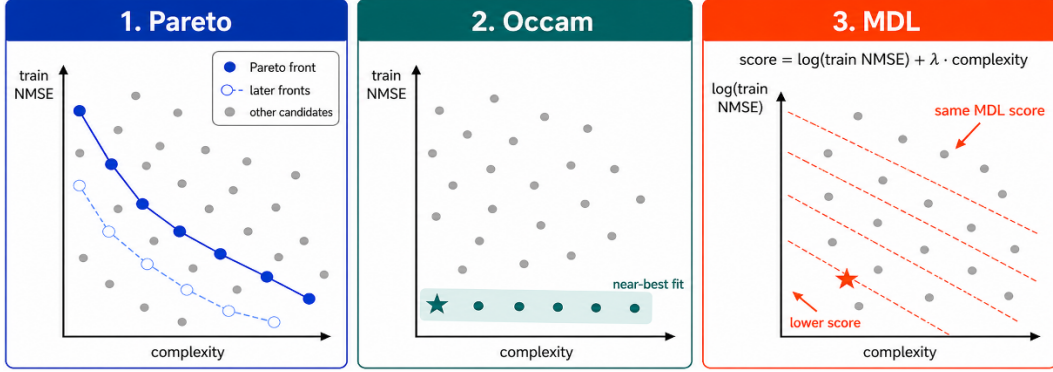


Figure 8: Complexity-aware final-candidate selection rules. Pareto treats each candidate as a point in training-NMSE-complexity space and selects from successive non-dominated fronts; Occam first keeps candidates with near-best training fit and then prefers simpler expressions; MDL combines training loss and complexity into a single scalar score. Details are provided in Appendix D1.

5 Discussion

To diagnose weaker MatSci results in Section 4, we identify two severe dataset identifiability issues. First, all 25 tasks use strain ϵ and temperature T , but the samples collapse to one dimension: across train, test, and OOD splits, $T \approx 273 + 500\epsilon$. Fitting $T = a + b\epsilon$ for each task and split gives correlations within 2.7×10^{-12} of one and a maximum absolute residual of 4.43×10^{-5} . This collinearity makes explicit temperature coupling unidentifiable, so structurally different expressions can achieve identical NMSE by replacing temperature-coupled terms with functions of ϵ alone. Figure 9 shows the residuals from this near-linear geometry. Second, Arrhenius-like factors vary too little to be reliably identified. Eight MatSci equations contain $\exp(-c/T)$ terms, but these factors change by 0.11%–2.06% on train/test and 0.006%–0.108% on OOD. In MatSci5, $\exp(-5.9485/T)$ changes from 0.978446 to 0.989105 on train and from 0.989106 to 0.989672 on OOD. Hence $e^p \exp(-c/T)$ behaves like a rescaled pure-strain term Ce^p , making the Arrhenius structure difficult to distinguish from a constant multiplier.

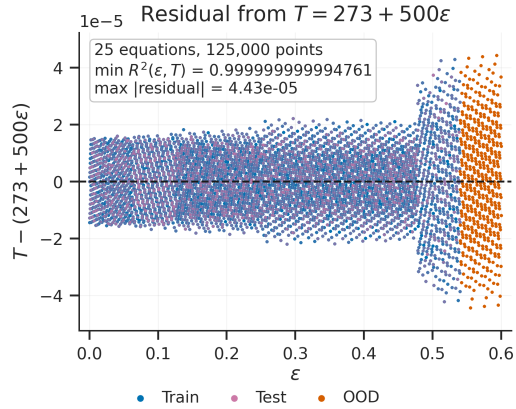


Figure 9: Residuals from the MatSci. Across train, test, and OOD samples, the maximum absolute residual is 4.43×10^{-5} .

In other dataset splits, the collinear issue is not dataset-wide as in MatSci, but individual tasks still exhibit strong pairwise dependence. Appendix D2 reports the 12 FunctionEvolve failure cases outside MatSci and shows that most still contain a variable pair with large R^2 . These dependencies can again weaken structural identifiability, because different symbolic mechanisms may become difficult to distinguish over the sampled trajectory even when the overall split is not globally degenerate.

Although our audit highlights limitations in LLM-SRBench and need for more reliable datasets, it remains the latest synthetic SR benchmark and reduces memorization risk relative to literature-derived benchmarks like AIFeynman[Udrescu and Tegmark, 2020]; constructing a new benchmark is beyond the scope of this work.

6 Conclusion

We introduced FunctionEvolve, an LLM-driven SR framework combining semantic initialization, diversity-aware selection, local mutation by AST rule and LLM proposal, and structure-aware coefficient optimization. On the 129-task synthetic subset of LLM-SRBench, FunctionEvolve recovers 107 exact symbolic forms with *Claude Opus 4.6*, substantially improving symbolic accuracy while preserving near-GT numerical precision; on the complementary 120-task AI-Feynman evaluation, it recovers the correct symbolic form for all 120 tasks as its top-1 prediction. Our ablations explain

why: LLM-extracted domain priors provide semantic guidance that steers the search toward plausible expressions, explicit AST structure organizes symbolic exploration, and structure-aware optimization prevents promising skeletons from being discarded due to poorly fitted constants.

Beyond these results, our audit identifies critical limitations in LLM-SRBench itself: the MatSci split has severe collinearity between T and ϵ , making key mechanisms unidentifiable and allowing structurally incorrect expressions to attain very low NMSE. Taken together, these findings suggest that progress in scientific SR requires joint attention to symbolic representation, coefficient fitting, and benchmark design. Open directions include dynamical systems without closed forms, larger candidate-variable sets, and benchmarks that are both reliable and realistic.

References

- Jean-Philippe Bruneton. Enhancing symbolic regression with quality-diversity and physics-inspired constraints, 2025. URL <https://arxiv.org/abs/2503.19043>.
- Bogdan Burlacu, Kaifeng Yang, and Michael Affenzeller. Population diversity and inheritance in genetic programming for symbolic regression. *Natural Computing*, 23, 01 2023. doi: 10.1007/s11047-022-09934-x.
- William La Cava, Patryk Orzechowski, Bogdan Burlacu, Fabrício Olivetti de França, Marco Virgolin, Ying Jin, Michael Kommenda, and Jason H. Moore. Contemporary symbolic regression methods and their relative performance, 2021. URL <https://arxiv.org/abs/2107.14351>.
- Miles Cranmer. Interpretable machine learning for science with PySR and SymbolicRegression.jl, 2023. URL <https://arxiv.org/abs/2305.01582>.
- Patrik D’haeseleer. Context preserving crossover in genetic programming. 1:256 – 261 vol.1, 07 1994. doi: 10.1109/ICEC.1994.350006.
- L. G. A dos Reis, V. L. P. S. Caminha, and T. J. P. Penna. Benchmarking symbolic regression constant optimization schemes, 2024. URL <https://arxiv.org/abs/2412.02126>.
- Mengge Du, Yuntian Chen, Zhongzheng Wang, Longfeng Nie, and Dongxiao Zhang. LLM4Ed: Large language models for automatic equation discovery, 2024. URL <https://arxiv.org/abs/2405.07761>.
- Arya Grayeli, Atharva Sehgal, Omar Costilla-Reyes, Miles Cranmer, and Swarat Chaudhuri. Symbolic regression with a learned concept library, 2024. URL <https://arxiv.org/abs/2409.09359>.
- Zelin Guo, Siqi Wang, Yonglin Tian, Jing Yang, Hui Yu, Xiaoxiang Na, Levente Kovacs, Li Li, Petros A. Ioannou, and Fei-Yue Wang. SR-LLM: An incremental symbolic regression framework driven by LLM-based retrieval-augmented generation. *Proceedings of the National Academy of Sciences*, 122(52):e2516995122, 2025. doi: 10.1073/pnas.2516995122.
- Michael Kommenda, Bogdan Burlacu, Gabriel Kronberger, and Michael Affenzeller. Parameter identification for symbolic regression using nonlinear least squares. *Genetic Programming and Evolvable Machines*, 21, 09 2020. doi: 10.1007/s10710-019-09371-3.
- John R. Koza. Genetic programming as a means for programming computers by natural selection. *Statistics and Computing*, 4(2):87–112, June 1994. ISSN 1573-1375. doi: 10.1007/BF00175355. URL <https://doi.org/10.1007/BF00175355>.
- Stefan Kramer, Mattia Cerrato, Jannis Brugger, Sašo Džeroski, and Ross King. Automated scientific discovery: From equation discovery to autonomous discovery systems, 2023. URL <https://arxiv.org/abs/2305.02251>.
- Robert Tjarko Lange, Yuki Imajuku, and Edoardo Cetin. ShinkaEvolve: Towards open-ended and sample-efficient program evolution, 2025. URL <https://arxiv.org/abs/2509.19349>.
- Pat Langley. Data-driven discovery of physical laws. *Cognitive Science*, 5(1):31–54, 1981. doi: <https://doi.org/10.1111/j.1551-6708.1981.tb00869.x>. URL <https://onlinelibrary.wiley.com/doi/abs/10.1111/j.1551-6708.1981.tb00869.x>.

- Qiang Lu, Jun Ren, and Zhiguang Wang. Using genetic programming with prior formula knowledge to solve symbolic regression problem. *Computational Intelligence and Neuroscience*, 2016:1–17, 12 2015. doi: 10.1155/2016/1021378.
- Georg Martius and Christoph H. Lampert. Extrapolation and learning equations, 2016. URL <https://arxiv.org/abs/1610.02995>.
- David J. Montana. Strongly typed genetic programming. *Evolutionary Computation*, 3(2):199–230, Summer 1995. ISSN 1063-6560. doi: 10.1162/evco.1995.3.2.199. URL <http://vishnu.bbn.com/papers/stgp.pdf>.
- T. Nathan Mundhenk, Mikel Landajuela, Ruben Glatt, Claudio P. Santiago, Daniel M. Faissol, and Brenden K. Petersen. Symbolic regression via neural-guided genetic programming population seeding, 2021. URL <https://arxiv.org/abs/2111.00053>.
- Alexander Novikov, Ngãn Vũ, Marvin Eisenberger, Emilien Dupont, Po-Sen Huang, Adam Zsolt Wagner, Sergey Shirobokov, Borislav Kozlovskii, Francisco J. R. Ruiz, Abbas Mehrabian, M. Pawan Kumar, Abigail See, Swarat Chaudhuri, George Holland, Alex Davies, Sebastian Nowozin, Pushmeet Kohli, and Matej Balog. AlphaEvolve: A coding agent for scientific and algorithmic discovery, 2025. URL <https://arxiv.org/abs/2506.13131>.
- Brenden K. Petersen, Mikel Landajuela, T. Nathan Mundhenk, Claudio P. Santiago, Soo K. Kim, and Joanne T. Kim. Deep symbolic regression: Recovering mathematical expressions from data via risk-seeking policy gradients, 2021. URL <https://arxiv.org/abs/1912.04871>.
- Subham S. Sahoo, Christoph H. Lampert, and Georg Martius. Learning equations for extrapolation and control, 2018. URL <https://arxiv.org/abs/1806.07259>.
- Michael Schmidt and Hod Lipson. Distilling free-form natural laws from experimental data. *Science*, 324(5923):81–85, 2009.
- Asankhaya Sharma. OpenEvolve: an open-source evolutionary coding agent, 2025. URL <https://github.com/algorithmicsuperintelligence/openevolve>.
- Parshin Shojaee, Kazem Meidani, Shashank Gupta, Amir Barati Farimani, and Chandan K Reddy. LLM-SR: Scientific equation discovery via programming with large language models. *arXiv preprint arXiv:2404.18400*, 2024.
- Parshin Shojaee, Ngoc-Hieu Nguyen, Kazem Meidani, Amir Barati Farimani, Khoa D Doan, and Chandan K Reddy. LLM-SRBench: A new benchmark for scientific equation discovery with large language models, 2025. URL <https://arxiv.org/abs/2504.10415>.
- Silviu-Marian Udrescu and Max Tegmark. AI Feynman: A physics-inspired method for symbolic regression. *Science Advances*, 6(16):eaay2631, 2020. doi: 10.1126/sciadv.aay2631. URL <https://www.science.org/doi/abs/10.1126/sciadv.aay2631>.
- Marco Virgolin and Solon P. Pissis. Symbolic regression is NP-hard, 2022. URL <https://arxiv.org/abs/2207.01018>.
- Boxiao Wang, Kai Li, Tianyi Liu, Chen Li, Junzhe Wang, Yifan Zhang, and Jian Cheng. LLM-based scientific equation discovery via physics-informed token-regularized policy optimization, 2026. URL <https://arxiv.org/abs/2602.10576>.
- Runxiang Wang, Boxiao Wang, Kai Li, Yifan Zhang, and Jian Cheng. DRSR: LLM-based scientific equation discovery with dual reasoning from data and experience, 2025. URL <https://arxiv.org/abs/2506.04282>.
- P. A. Whigham. Grammatically-based genetic programming. In Justinian P. Rosca, editor, *Proceedings of the Workshop on Genetic Programming: From Theory to Real-World Applications*, pages 33–41, Tahoe City, California, USA, 9 July 1995. URL <http://divcom.otago.ac.nz/sirc/Peterw/Publications/ml95.zip>.
- Shijie Xia, Yuhan Sun, and Pengfei Liu. SR-Scientist: Scientific equation discovery with agentic AI, 2025. URL <https://arxiv.org/abs/2510.11661>.

A Code and Data Availability

We provide an anonymized repository containing the FunctionEvolve implementation, experiment configuration files, prompt templates, scripts for running the main experiments and baselines, and raw result files used to produce the tables and figures in this paper. The repository also includes environment setup instructions, benchmark data access and preparation instructions, and command-line examples for reproducing the main LLM-SRBench experiments and ablations: <https://github.com/Phoinikas03/FunctionEvolve>.

The existing benchmark and baseline assets used in our experiments are credited in the main text and are publicly available from their official repositories. LLM-SRBench and its associated LLM-SR benchmark code are available under the MIT license at <https://github.com/deep-symbolic-mathematics/llm-srbench>; OpenEvolve is available under the Apache-2.0 license at <https://github.com/algorithmicsuperintelligence/openevolve>. The AI-Feynman benchmark is available from the official download page: <https://space.mit.edu/home/tegmark/aifeynman.html>.

The main LLM-SRBench evaluation uses the 129-task synthetic subset, covering four scientific domains: biology/population growth, chemistry/reaction kinetics, physics/oscillation, and materials science. For the AI-Feynman evaluation in Section 4.2, we use the full benchmark family consisting of the 100 original Feynman equations and the 20 bonus equations, for a total of 120 tasks. Symbolic matches are judged against the benchmark target expressions over the benchmark-specified variable domains. Thus, domain-restricted identities are counted as matches when the candidate and target agree throughout the stated domain; equivalence outside that domain is not required.

B Resource Usage

The main LLM-SRBench comparisons, ablations, and rerun baselines use the same 129-task synthetic subset. For the baseline reruns, we follow the public LLM-SR and OpenEvolve implementations and keep their released search and evaluator hyperparameters unchanged, rather than tuning them for FunctionEvolve. Concretely, FunctionEvolve runs for at most 30 evolution iterations per task, OpenEvolve runs for 200 iterations per task, and LLM-SR runs with a 1000-sample budget per task.

B1 LLM Usage

LLM call accounting. Both the *Claude Opus 4.6* and *GPT-5.2-medium* experiments are run through external LLM APIs. Unless otherwise stated, the accounting below uses the complete full-setting *Claude Opus 4.6* logs over the 129 LLM-SRBench tasks.

In each FunctionEvolve evolution iteration, the Selector chooses 5 candidate expressions as parents, and the LLM Mutator proposes 20 new candidate expressions for each selected parent. Search terminates early once 50 mature expressions are found, where maturity is defined by training NMSE falling below the task-specific threshold. Retries are used only when parsing or validation fails.

For the baselines, LLM-SR generates one new candidate expression per sample, and OpenEvolve generates one new child program per iteration. Table B1 reports the theoretical maximum number of LLM calls; actual usage can differ slightly because of early stopping, retry, or logging behavior. Figure 10 and Table B2 summarize the observed call counts.

The observed call counts show that FunctionEvolve uses substantially fewer LLM requests than the baseline search loops. Although its theoretical per-task budget is 182 calls, early stopping reduces the average to 66.86 calls per task. Most of these calls are spent on the LLM Mutator, which averages 53.80 calls per task, while the Selector averages 11.06 calls and the Generator is fixed at 2 calls. In contrast, LLM-SR stays close to its 1000-iteration budget, and OpenEvolve stays close to its 200-iteration budget. Thus, FunctionEvolve reaches its main results with about 15x fewer LLM calls than LLM-SR and about 3x fewer calls than OpenEvolve on average.

Table B1: Theoretical maximum per-task LLM-call budget for FunctionEvolve and the LLM-driven baselines.

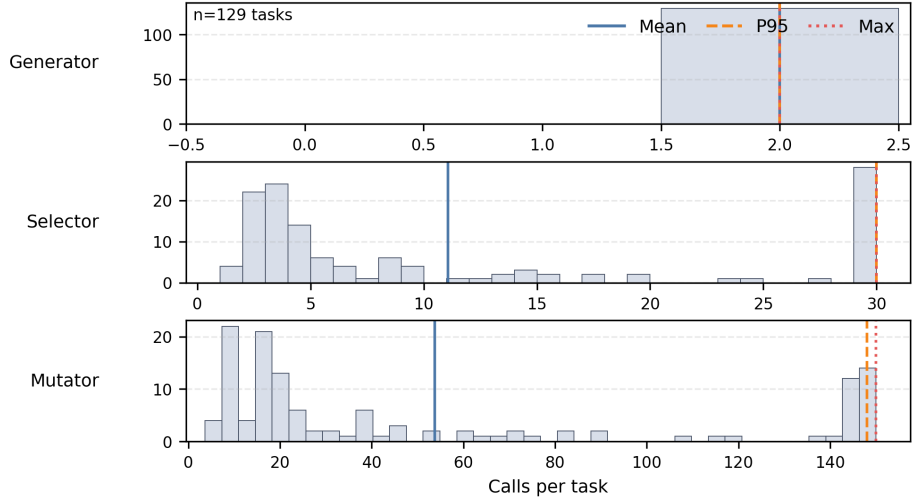


Figure 10: Component-wise distributions of LLM call counts over 129 complete task logs from the full *Claude Opus 4.6* FunctionEvolve experiment. Vertical lines mark the mean, 95th percentile, and maximum per-task call count for each main search component.

Method/component	Trigger	Maximum call budget per task
FunctionEvolve		
Generator	Domain-prior extraction and seed initialization	2 calls
Selector	Once per evolution round	≤ 30 calls
LLM Mutator	Once per selected parent	$\leq 30 \times 5 = 150$ calls
LLM-SR	One child hypothesis per iteration	1000 calls
OpenEvolve	One child hypothesis per iteration	200 calls

Table B2: LLM call usage on the 129-task LLM-SRBench subset under *Claude Opus 4.6*.

Method/component	Total calls	Mean/task	Std./task	Median	P95	Max
FunctionEvolve	8625	66.86	64.88	30	180	182
Generator	258	2.00	0.00	2	2	2
Selector	1427	11.06	11.08	5	30	30
LLM Mutator	6940	53.80	53.80	23	148	150
LLM-SR	129035	1000.27	3.07	1001	1001	1001
OpenEvolve	25994	201.50	2.11	200	205	206

LLM token accounting. We follow the same accounting protocol as the LLM call accounting. Table B3 reports the aggregate prompt, completion, and total token counts, and Figure 11 shows the per-task token distribution for the three FunctionEvolve LLM components, separating input and output tokens.

The token accounting shows a different tradeoff from the call accounting. FunctionEvolve uses fewer LLM calls than both LLM-SR and OpenEvolve, but each call is longer because the Selector observes the evolving tree summary and the LLM Mutator receives rich structural context. As a result, FunctionEvolve uses 340.36M total tokens, compared with 262.16M for LLM-SR and 244.79M for OpenEvolve. Within FunctionEvolve, token usage is highly concentrated in the Selector: it accounts for 290.44M tokens, or 85.33% of the FunctionEvolve total, while the LLM Mutator accounts for 49.07M tokens and the Generator for only 0.85M. Figure 11 shows that per-task token usage varies mainly in the Selector and LLM Mutator, while the Generator remains nearly constant across tasks because it is used only for initialization. Since prompt tokens are much cheaper than completion tokens in typical LLM pricing, we also report a price-weighted cost proxy in Table B3, computed as prompt tokens/5 plus completion tokens. Under this weighting, FunctionEvolve costs 85.56M

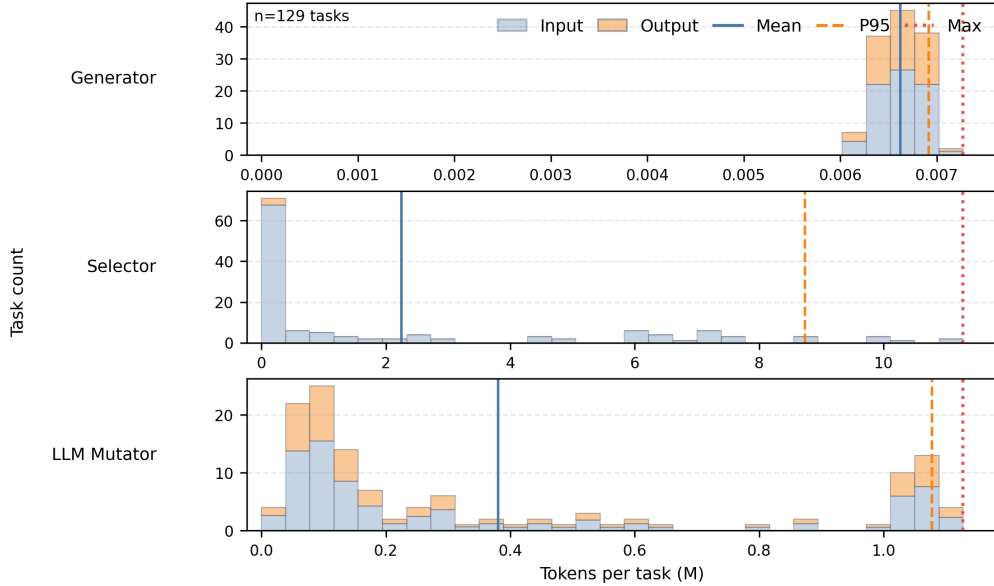


Figure 11: Per-task token-usage distributions for the three main FunctionEvolve LLM components under *Claude Opus 4.6*. Each row is a histogram over the 129 tasks; each bin is split into input-token and output-token contributions. Vertical lines mark the mean, 95th percentile, and maximum total tokens per task for the corresponding component.

output-token equivalents, lower than LLM-SR’s 143.45M and comparable to OpenEvolve’s 68.13M despite using more total tokens.

Table B3: Observed token usage on the 129-task LLM-SRBench subset under *Claude Opus 4.6*. Token counts and price-weighted costs are reported in millions. The weighted-cost column assumes one prompt token costs one fifth of one completion token.

Method/component	Prompt tokens	Completion tokens	Total tokens	Weighted cost
FunctionEvolve	318.50	21.86	340.36	85.56
Generator	0.50	0.35	0.85	0.45
Selector	288.86	1.58	290.44	59.35
LLM Mutator	29.14	19.93	49.07	25.76
LLM-SR	148.40	113.77	262.16	143.45
OpenEvolve	220.83	23.96	244.79	68.13

B2 CPU Usage

All local computation was performed on modern multicore CPU servers with heterogeneous configurations, each providing at least 64 logical CPUs. The local CPU workload consists primarily of candidate validation, program or expression execution, coefficient optimization, and post-fit screening. The existing logs do not record process-level user/system CPU time or instantaneous utilization; therefore, we report observed wall-clock time, evaluator parallelism, candidate-evaluation counts, and timeout behavior rather than exact CPU-hours.

This hardware lower bound is important for interpreting wall-clock cost. The original LLM-SR loop generates one offspring from one parent at each iteration, and OpenEvolve similarly evaluates one child program per iteration. FunctionEvolve instead selects multiple parents and expands them into a batch of candidate expressions. Although the full setting evaluates 126.09 offspring per round on average, these evaluations are independent and can be distributed across modern multicore CPUs; consequently, wall-clock time does not increase in proportion to the number of candidates, while one-offspring baselines leave much of this parallelism unused.

Table B4: CPU-evaluation protocol for FunctionEvolve and the LLM-driven baselines. Retry counts refer to local evaluator retries, not LLM API retries.

Method	Offspring per round	Evaluator	Timeout	Retries
FunctionEvolve	100 LLM proposals + rule mutations (mean: 126.09)	Structure-aware coefficient optimizer	120 s	0
LLM-SR	1 candidate per sample	BFGS optimizer	30 s	0
OpenEvolve	1 child program per iteration	BFGS optimizer	90 s	3*

*OpenEvolve retries evaluation exceptions up to three times; evaluator timeouts are returned directly as timeout results.

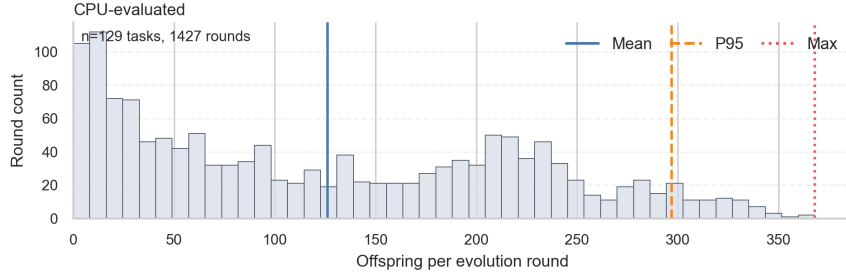


Figure 12: Distribution of CPU-evaluated offspring counts per FunctionEvolve round over 129 complete full-run task logs. Counts include candidates that remain after structural deduplication and parameter-count filtering and therefore enter coefficient optimization. Vertical lines mark the mean, 95th percentile, and maximum.

Table B4 summarizes the local CPU-evaluation protocol. In FunctionEvolve, the 100 LLM-proposed offspring in each round come from 5 LLM Mutator calls over 5 selected parents, and deterministic rule mutations add further non-LLM offspring. The resulting batch-size distribution is shown in Figure 12. Using the most conservative 64-logical-CPU reference, the mean batch size corresponds to roughly $126.09/64 = 1.97$ candidate-equivalent parallel waves, making the local wall-clock evaluation load comparable to the one-offspring baseline steps up to scheduling and optimizer-runtime variation.

B3 GPU Usage

GPU resources were used only for local LLM inference, not for symbolic candidate execution, coefficient optimization, or post-fit screening. The locally served *Llama-3.1-8B*, *Qwen3.6-27B*, and *DeepSeek-V4-Pro* inference endpoints were deployed on 16 NVIDIA H20-3e data-center AI accelerators with CUDA 13.1 and 144 GiB HBM per card.

These GPU resources should therefore be interpreted as serving hardware for the local LLM backbones, which were served with vLLM 0.20.0 for inference. The CPU accounting in Appendix B2 remains the relevant local compute description for expression evaluation and fitting, while externally hosted LLMs such as *Claude Opus 4.6* are represented only through the call and token accounting in Appendix B1.

C Additional Details of FunctionEvolve

C1 Algorithmic Procedure

Operational subroutines **RULEADDITION** is a deterministic parent-level expansion. For a selected parent p , it attaches the elementary content library in Table 1 through $p + g$, $p \cdot g$, division templates, and unary wraps. There is no blanket preprocessing stage applied to all seeds or all offspring; each generated candidate corresponds to one explicit mutation step.

DEGENERACYCHECK is a deterministic state-management routine that decides whether an evaluated candidate remains active. It returns $\delta_g \in \{\text{OK}, \text{SIMPLIFIED}, \text{OVERFIT}, \text{TIMEOUT}\}$. It marks deep expressions with abnormal fitted coefficients ($|c_j| > 10^3$) as **OVERFIT**, applies constant-induced

FunctionEvolve

```

Input          LLM modules  $\pi_G, \pi_S, \pi_M$ , dataset  $\mathcal{D} = \{(\mathbf{x}_i, y_i)\}_{i=1}^n$  with task-level context  $T$ 
Output       Ranked symbolic expressions with fitted constants and scores

# Initialization by Generator
 $\mathcal{K} \leftarrow \pi_G.\text{KNOWLEDGE}(T, \mathcal{D})$ 
 $\mathcal{S}_0 \leftarrow \pi_G.\text{SEEDS}(T, \mathcal{D}, \mathcal{K})$ 
 $\mathcal{E} \leftarrow \emptyset, \mathcal{H} \leftarrow \emptyset$ 

for  $f \in \mathcal{S}_0$  do
|    $f, \Theta \leftarrow \text{NORMALIZE}(f)$ 
|    $s, \hat{c} \leftarrow \text{OPTIMIZER}(f, \Theta, \mathcal{D})$ 
|    $\mathcal{E} \leftarrow \mathcal{E} \cup \{(f, \Theta, \hat{c}, s, \text{root})\}$ 
end for

# Evolution over the expression tree
while stopping criterion is not met do
|    $\mathcal{Z} \leftarrow \text{TREESUMMARY}(\mathcal{E}, \mathcal{H})$ 
|    $\mathcal{P} \leftarrow \pi_S.\text{SELECTPARENTS}(\mathcal{Z}, T)$ 
|    $\mathcal{C} \leftarrow \emptyset$ 
|   for  $p \in \mathcal{P}$  do
|   |    $\mathcal{A} \leftarrow \text{RULEADDITION}(p) \cup \text{RULEDELETION}(p)$ 
|   |    $\mathcal{L} \leftarrow \pi_M.\text{MUTATE}(p, \text{AST}(p), \mathcal{A}, \mathcal{K}, \mathcal{Z})$ 
|   |    $\mathcal{C} \leftarrow \mathcal{C} \cup \{(g, p) : g \in \text{NORMALIZEDDEDUP}(\mathcal{A} \cup \mathcal{L})\}$ 
|   |   end for
|   |   for  $(g, p) \in \mathcal{C}$  do
|   |   |    $g, \Theta_g \leftarrow \text{NORMALIZE}(g)$ 
|   |   |   if  $\text{VALID}(g, \Theta_g, \mathcal{E})$  then
|   |   |   |    $s_g, \hat{c}_g \leftarrow \text{OPTIMIZER}(g, \Theta_g, \mathcal{D})$ 
|   |   |   |    $\delta_g, \tilde{g}, \tilde{\Theta}_g \leftarrow \text{DEGENERACYCHECK}(g, \Theta_g, \hat{c}_g)$ 
|   |   |   |    $\mathcal{E} \leftarrow \mathcal{E} \cup \{(g, \Theta_g, \hat{c}_g, s_g, \text{parent} = p, \delta_g)\}$ 
|   |   |   |   if  $\delta_g = \text{SIMPLIFIED}$  then  $\mathcal{C} \leftarrow \mathcal{C} \cup \{(\tilde{g}, g)\}$  end if
|   |   |   |   end if
|   |   |   end for
|   |    $\mathcal{H} \leftarrow \mathcal{H} \cup \mathcal{P}; \text{ MARKMATURE}(\mathcal{E})$ 
|   end while
return  $\text{TOPEXPRESSIONS}(\mathcal{E})$ 

```

simplifications such as zeroing small multiplicative terms, snapping near-rational exponents, simplifying $\exp(0)$ and $\log(1)$, reducing simple trigonometric degeneracies, and merging nearly identical nonlinear terms. If the simplification removes all feature variables or creates infinity, the candidate is marked OVERFIT; if it yields a different valid expression, the original evaluated candidate is marked SIMPLIFIED and the simplified expression is reinserted as its descendant for normal normalization, deduplication, and optimization. Timeouts are conservatively treated as OK.

These flags directly control the search tree. Nodes with $\delta_g \neq \text{OK}$ are kept only as evaluated audit records and are excluded from the Selector’s tree summary, so they cannot become future parents. MARKMATURE marks an active evaluated node as mature once its training NMSE is below τ_{train} . Mature nodes may still be selected for a small annealing budget; after that budget is exhausted, they are removed from the Selector context. The run stops early after the configured number of mature nodes has been collected. TOPEXPRESSIONS returns mature nodes, supplemented if needed by non-mature evaluated nodes, ordered by training NMSE. Test and OOD NMSE are logged for post-hoc reporting only and are not exposed to the Selector or Mutator during search.

Full-run configuration Table C1 lists the command-line configuration used by `run.sh full`; unspecified arguments use the defaults in `main.py`.

C2 Generator

Procedure The Generator is used during the one-shot initialization stage. It has two LLM-facing subroutines. First, `generate_domain_knowledge` reads the task context and available variables, infers either the scientific domain or, for dimension-only tasks such as AI-Feynman entries without natural-language background, a dimension-aware structural prior. It returns formulae priors and heuristic structural cues. These LLM-proposed priors are combined with a fixed catalog of generic

Table C1: `run.sh` full configuration for the full FunctionEvolve setting.

Parameter	Meaning	Value
<code>-optimizer</code>	Constant-fitting backend	Structure
<code>-max-steps</code>	Maximum evolutionary iterations per task	30
<code>-n-seeds</code>	Number of Generator seed expressions	20
<code>-candidate-num</code>	Number of parents selected per iteration	5
<code>-selector-context-size</code>	Maximum number of active nodes shown to the Selector	200
<code>-max-mature-nodes</code>	Early-stop target number of training-NMSE mature nodes	50
<code>-overfit-min-depth</code>	Minimum SymPy AST depth for large-coefficient overfit screening	10
<code>-equation-workers</code>	Active equation-level workers in full mode	10
<code>-n-eval-workers</code>	Local child-evaluation workers when no shared global worker pool is used	16 (default)
<code>-timeout</code>	Per-task wall-clock timeout shared by normalization, evaluation, degeneracy check, and optimizer	120 s (default)
<code>-refine-output</code>	Final parent-selection sweep for mature/supplement nodes	disabled in full; enabled only by <code>refine_full</code>
<code>-data-dir</code>	LLM-SRBench data directory	optional; defaults to dataset loader path unless provided

scientific laws or dimension/variable-name templates, so the downstream search receives both broad priors and task-specific or metadata-specific priors.

Second, `initialize_seeds` uses the task context, variables, and extracted knowledge to generate the initial expression pool. The seed prompt asks for diverse structures spanning both compact monomial/product/ratio/composition forms and multi-term sums, with roughly half generic elementary-function structures and half knowledge-informed structures. Each response must be a JSON array of SymPy-parseable expressions together with the parameter placeholders used in the expression. The implementation validates the JSON schema, parses each expression with SymPy, checks that free symbols come only from dataset variables or listed `c0, c1, ...` constants, and requires the listed constants to match those actually used. If LLM generation yields too few valid seeds, a fixed fallback seed list supplements the pool.

Table C2: Generator configuration used by the *Claude Opus 4.6* full run. Component-specific overrides are read from `opus-4-6.yaml`.

Parameter	Meaning	Value
<code>n_seeds</code>	Number of initial seed expressions	20
<code>generator.temperature</code>	Default Generator decoding temperature	1.0
<code>domain_knowledge.temperature</code>	Domain-knowledge extraction temperature	0.7
<code>seed_generation.temperature</code>	Seed-expression generation temperature	0.9
<code>describe_batch.temperature</code>	Batch-description temperature	0.5
<code>max_tokens</code>	Maximum response length for Generator subroutines	128000

Degenerated Generator For ablations, FunctionEvolve can replace the LLM Generator with a deterministic `MockGenerator`. In this mode, no LLM calls are made: domain knowledge is empty and initial expressions are drawn from a fixed fallback list. This isolates the contribution of LLM-based initialization and domain-prior extraction from the rest of the search pipeline.

Prompting interface The Generator uses separate prompt interfaces for domain knowledge extraction and seed expression initialization. The prompt boxes below show the interfaces used by these subroutines in abbreviated form. The domain knowledge prompt returns a JSON object,

while the seed prompt returns a JSON array. In both cases, the implementation requests JSON-only output, optionally attaches a guided JSON schema when the backend supports it, extracts a JSON block if one is present, and validates the parsed result before it is inserted into the search state. The same seed-generation interface is used across LLM-SRBench and AI-Feynman; for AI-Feynman tasks without natural-language background, only the domain-knowledge stage switches to a dimension/variable/range-aware variant, and the seed prompt labels the knowledge-informed half as dimension/variable-informed formulas.

Generator domain-knowledge system prompt

```
You are a cross-disciplinary mathematical modeling expert, proficient in
→ classical formulas and mathematical models from physics, chemistry,
→ biology, engineering, economics, and other fields.

Given a background description of a symbolic regression task (including
→ variable names and their physical meanings), please:
1. Analyze the most likely scientific domain/sub-domain for this task
2. List classical formula structures related to these variables in that
→ domain

## Output Format
Return only a JSON object:
{"domain": "<domain name>", "analysis": "<1-2 sentence domain analysis>",
→ "formulas": [...], "heuristics": [...]}

- domain: The scientific domain this task belongs to.
- analysis: Briefly explain why it belongs to this domain and the possible
→ physical relationships between variables.
- formulas: List 5~15 common formula structural patterns in this domain. Use
→ actual variable names when possible, arrange from simple to complex,
→ include domain-specific function forms, and write each entry as "Name:
→ formula form (applicable scenario)".
- heuristics: List 5~10 domain-specific formula-structure heuristic features
→ describing what physical behavior corresponds to what mathematical
→ structure.

Constant notation convention: constant parameters must appear in
→ multiplicative form and must not be placed in the denominator. Use `c *
→ var` rather than `var / c`.
```

Generator domain-knowledge user prompt

```
{context}

Available variables: {variables}

Please analyze the scientific domain of this task and list common formula
→ structures related to these variables in that domain.
```

Generator seed system prompt

```
You are a symbolic-regression expert. Generate diverse candidate closed-form
→ formulas for the dataset described below, to seed an evolutionary search.

## Structural Prior
The ground-truth formula may be EITHER:
- a single compact monomial / product / ratio / composition, such as
→ `c0*x1*x2/x3` or `c0*exp(-c1*x**2)`; OR
- a sum of several terms, such as `c0*x + c1*x**2 + c2`.
Your seed set MUST cover both archetypes.
```

```

## Building Blocks
power `x*c`, trigonometric `sin`/`cos`, exponential `exp`, logarithmic
↪ `log(1+x)`, `sqrt`, and, where physically meaningful, `Abs(x)` and
↪ `Max(x, 0)`.

## Using {knowledge_basis}
{domain_knowledge}

## Constant Notation Convention
Constant parameters should always appear in multiplicative form, never alone
↪ in a denominator: write `c0*x` and `c0/(x + c1)`, not `x/c0`.

## Task Background
{context}

## Available Variables
{variables}

Please generate {n_seeds} candidate formulas with different structures at
↪ once, and return only a JSON array:
[{"expression": "...", "params": ["c0", "c1"]}, ...]

```

Generator seed user prompt

```

Based on the above task metadata, generate {n_seeds} candidate formulas with
↪ diverse structures.

## Requirements
Formulas must cover both of the following categories, arranged from simple to
↪ complex:

A. Basic function structures (approximately half): Include BOTH compact
↪ single-term shapes (monomial/product/ratio/composition) AND multi-term
↪ sums. Ensure at least one variant of each basic type:
- Monomial / product:  $c0*x1*x2$ ,  $c0*x1*x2/x3$ 
- Power-law / composition:  $c0*x**c1$ ,  $c0*exp(-c1*x**2)$ ,  $c0/sqrt(1 -$ 
↪  $x**2/c1**2)$ 
- Linear:  $c0*x + c1$ 
- Quadratic/polynomial:  $c0*x**2 + c1*x + c2$ 
- Non-integer power law:  $c0*x**c1$ 
- Exponential:  $c0*exp(c1*x)$ 
- Logarithmic:  $c0*log(1 + c1*x)$ 
- Rational:  $c0*x/(x + c1)$ 
- Trigonometric:  $c0*sin(c1*x)$ 
- Hyperbolic:  $c0*tanh(c1*x + c2)$ 
- Square root:  $c0*sqrt(x**2 + c1)$ 
- Simple combinations of the above basic types

B. Knowledge-informed formulas (approximately half): Based on the task
↪ background and the domain-knowledge or dimension/variable-name structures
↪ listed above, generate formula forms most likely to match the data.

Note: All constants in formulas must be represented as  $c0$ ,  $c1$ ,  $c2\dots$ , and
↪ variables must use names from the available variables list.

```

1 C3 Evolutionary Tree Search

2 FunctionEvolve maintains the search state as an evolutionary tree rather than as an unstructured
3 pool of candidate expressions. Each node in the tree corresponds to a symbolic expression together
4 with its associated search state, while edges record parent-child relations induced by mutation. This
5 representation preserves structural lineage throughout the search and allows the system to summarize
6 the current search frontier for downstream selection.

Table C3: Main information maintained for each node in the evolutionary tree. The last column indicates whether the field itself, or a derived summary of it, is visible to the Selector.

Field	Type	Description	Selector visibility
<code>id</code>	string	Identifier for this node.	Yes
<code>formula</code>	string	Canonical symbolic expression string.	Yes
<code>parent_id</code>	string / None	Identifier of the parent node in the evolutionary tree.	Yes
<code>train_nmse</code>	float / None	Training NMSE after constant fitting.	Yes
<code>test_nmse</code>	float / None	Test NMSE maintained for evaluation.	No
<code>ood_test_nmse</code>	float / None	Out-of-distribution NMSE maintained for evaluation.	No
<code>is_evaluated</code>	bool	Whether the node has been evaluated after constant fitting.	No
<code>tree_depth</code>	integer	Depth of the parsed expression tree; exposed as <code>depth</code> .	Yes
<code>operator_counts</code>	dictionary	Counts of operator types in the expression tree; exposed to the Selector only through the aggregated field <code>n_operators</code> .	Yes
<code>ast_features</code>	structured features	Additional AST-derived structural features used internally.	No
<code>param_names</code>	list of strings	Names of tunable scalar parameters; exposed only through the aggregated field <code>n_params</code> .	Yes
<code>fitted_params</code>	list of floats	Optimized parameter values; exposed to the Selector as a formatted string when available.	Yes
<code>sympy_expr</code>	symbolic object	Parsed symbolic expression used for internal manipulation and analysis.	No

7 At a high level, the tree stores two types of information: the current set of candidate expressions
8 and the parent-child relations among them. Each node further maintains its own evaluation statistics,
9 structural information, and parameter-related information. Table C3 summarizes the main information
10 maintained for each node, together with whether it is visible to the Selector.

11 C4 Selector

12 **Procedure** At each search iteration, the Selector receives a compact summary of the current search
13 tree, together with the task context and the record of previously chosen parents. Based on this
14 information, it identifies a small set of parent expressions for further expansion and provides a brief
15 rationale for each choice. These selected parents are then forwarded to the subsequent mutation stage.
16 In this way, the Selector determines how the available search budget is allocated across competing
17 search directions.

Table C4: Selector configuration used in our experiments.

Parameter	Meaning	Value
<code>candidate_num</code>	Number of parents selected per iteration	5
<code>selector_context_size</code>	Maximum number of summarized active nodes visible to the Selector in <code>run.sh full</code>	200
<code>temperature</code>	Sampling temperature for <i>Claude Opus 4.6</i> Selector decoding	0.3
<code>max_tokens</code>	Maximum response length for Selector decoding	128000

19 **Visible node information** Although each tree node stores a full internal state, the Selector does
20 not access this state directly. Instead, it operates on the subset of per-node information marked as
21 visible in Table C3, together with the aggregated statistic `n_children`. In practice, this summary
22 provides information about predictive quality, structural complexity, local parameterization, and
23 search history, without exposing the full internal node state. Importantly, the summary contains only
24 training error. Test error and out-of-distribution error are maintained internally for evaluation, but are
25 never revealed to the Selector. This design prevents evaluation-time information from leaking into
26 the parent-selection process.

27 **Degenerated Selector** For ablations, FunctionEvolve supports two degenerated Selector variants.
28 The first variant replaces the LLM Selector with a deterministic `MockSelector`. This fallback ranks

29 evaluated nodes by numerical fitness and samples parents using a rank-based Boltzmann distribution,
30 so no LLM call is made during parent selection. The second variant keeps the LLM-based parent-
31 selection interface but removes AST-derived structural fields from the prompt, including parameter
32 count, tree depth, and operator count. This preserves LLM decision making while hiding explicit
33 AST structure, isolating the contribution of structural visibility in the Selector.

34 **Prompting interface** The exact prompt templates used by the Selector are shown below. The system
35 prompt defines the selection criteria and the required JSON-only output format, while the user prompt
36 template supplies the current tree summary and the historical selection records. The implementation
37 also attaches the same guided JSON schema when the backend supports it. The Selector uses the
38 same main template across datasets; AI-Feynman tasks append the dimension/variable/range task
39 background and a short instruction to prioritize formula quality, structural diversity, variable-name
40 cues, and dimensional metadata. For the ablation without AST-derived metadata, we use a variant
41 with the corresponding fields removed.

Selector system prompt

```
You are a strategic planning expert for symbolic regression search.

You will see a summary table of all generated formulas in the current
↪ evolution tree, each record contains:
- id          : Numeric unique identifier of the formula
- formula     : Formula in SymPy format
- train_nmse  : Training set NMSE = MSE/Var(Y) (None means not yet evaluated;
↪ lower is better, <1 is better than mean prediction)
- n_children  : Number of offspring this node has produced
- n_params    : Number of tunable parameters
- depth       : AST tree depth (nesting level; higher means deeper function
↪ nesting)
- n_operators : Total number of operator nodes in AST tree (higher means
↪ longer expression)
- fitted_params : Fitted parameter values (scientific notation)

Your task is to select {candidate_num} parent nodes for the next
↪ evolution iteration.
The system will automatically perform AST-based structural mutations (delete
↪ subtrees, add new terms, etc.) on each parent to generate multiple
↪ candidate offspring.

Please consider the following when selecting:
1. Structural simplicity first: Do not simply select the nodes with the
↪ lowest NMSE. Prefer structurally simple nodes (fewer n_params, shallower
↪ depth, fewer n_operators) that already have relatively low NMSE (e.g.,
↪ ~1e-3 order) - simple good formulas are more likely to produce meaningful
↪ improvements through mutation, while low NMSE in complex formulas often
↪ comes from overfitting
2. Algebraic structure diversity: The selected {candidate_num} parents
↪ should cover different algebraic structures as much as possible (e.g.,
↪ polynomial, power law, exponential, trigonometric, rational, etc.),
↪ avoiding highly similar formulas. Diverse starting points enable more
↪ comprehensive exploration of the search space
3. NMSE performance: When structures are similar, prefer nodes with lower
↪ NMSE that still have room for improvement
4. Number of offspring (n_children): If a node already has many offspring
↪ (e.g., n_children >= 5), it means that direction has been sufficiently
↪ explored; prefer nodes with fewer offspring
5. Historical selection records: Refer to the historical parent selection
↪ records. If certain formula structures have been repeatedly selected as
↪ parents in recent rounds but NMSE has not significantly decreased, they
↪ should be temporarily shelved in favor of other directions; if certain
↪ structures have not been explored recently, encourage selecting them as
↪ parents to expand the search space
```

Return only a JSON array with exactly {candidate_num} objects. Use the
 ↪ numeric `id` shown in the node summary as `parent_id`; do not copy the
 ↪ formula string into `parent_id`.

Required JSON schema:

```
{
  "type": "array",
  "minItems": {candidate_num},
  "maxItems": {candidate_num},
  "items": {
    "type": "object",
    "required": ["parent_id", "rationale"],
    "additionalProperties": false,
    "properties": {
      "parent_id": {"type": "integer"},
      "rationale": {"type": "string"}
    }
  }
}
```

Example item format (shape only; your actual output must contain exactly
 ↪ {candidate_num} objects):

```
[
  {"parent_id": 12, "rationale": "<selection rationale 1>"},
  {"parent_id": 7, "rationale": "<selection rationale 2>"}
]
```

- rationale: short final reason for selecting this parent.

Selector user prompt

Current evolution tree node summary ({n_nodes} nodes total, sorted by
 ↪ train_nmse ascending):

{tree_summary}

Historical Parent Selection Records

{selection_history}

Please comprehensively analyze the above nodes and historical selection
 ↪ records, select {candidate_num} structurally diverse and concise parents,
 ↪ and output a JSON array.

42 C5 Mutator

43 **AST representation** Each symbolic expression is parsed into a SymPy abstract syntax tree (AST),
 44 where internal nodes correspond to operators such as Add, Mul, Pow, exp, log, and sin, and leaf
 45 nodes correspond to variables or scalar parameters. For each expression f , we extract depth-aware
 46 structural features of the form

$$\mathcal{F}(f) = \{\text{Op}(\text{Depth} : k) \mid \text{Op is the operator type of a node and } k \text{ is its depth}\}.$$

47 For example, the expression $c_0x^{c_1} + c_2 \exp(c_3x)$ contains features such as Add(Depth:0),
 48 Mul(Depth:1), Pow(Depth:2), and exp(Depth:2).

49 **Rule-based mutations** The AST-rule Mutator applies deterministic edits directly on the expression
 50 tree. We use two classes of rule-based mutations. The first class performs deletion and simplification
 51 operations, including removing one term from an Add node, removing one non-numeric factor from
 52 a Mul node, unwrapping elementary functions such as $\exp(g) \mapsto g$, $\log(g) \mapsto g$, and $\sin(g) \mapsto g$,
 53 and reducing powers such as $x^n \mapsto x$. These operations are recursively applied to valid subtrees and
 54 remove candidates that do not contain feature variables.

55 The second class performs broad template-based addition. Given a parent expression f , the Mutator
 56 first defines an elementary content library g using the families in Table 1. It then enumerates $f + g$
 57 additive terms, $f \cdot g$ multiplicative factors, division templates, and unary wraps $\phi(cf)$ or f^c . In
 58 implementation, division uses the numerically stable subset $f/(1 + g_s)$ with g_s instantiated from
 59 linear, power, exponential, and logarithmic content, so the edit remains local to the parent and
 60 avoids bare learned constants in denominators. We intentionally keep this rule library generic and
 61 domain-agnostic to reduce dataset-specific overfitting, leaving richer structural refinements to the
 62 LLM-guided channel. For multivariate problems, the pair rational and power-law coupling families
 63 are instantiated over up to six ordered variable permutations, while single-variable families are
 64 instantiated over each feature variable.

65 **Normalization and deduplication** To reduce redundant candidates, we define a parameter-name-
 66 invariant structural fingerprint $\kappa(f)$. The fingerprint is constructed by recursively replacing all
 67 scalar parameter symbols in the AST with a shared placeholder, sorting the children of commutative
 68 operators such as Add and Mul, and serializing the resulting normalized tree. Expressions with the
 69 same fingerprint are treated as structurally equivalent up to parameter renaming.

70 After mutation, candidates are further normalized before evaluation. The normalization procedure
 71 applies algebraic simplifications, merges redundant scalar parameters, completes elementary-function
 72 parameterizations when necessary, and renumbers parameters in order of appearance as c_0, c_1, c_2, \dots
 73 Examples include rewriting $\exp(A + c)$ as $c' \exp(A)$, rewriting $\exp(c \log g)$ as g^c , simplifying
 74 $\log(\exp(g))$ to g , and merging products or sums of scalar parameters into a single parameter.

75 **LLM-guided mutations** In addition to rule-based mutations, the LLM Mutator proposes non-
 76 template structural refinements for each parent expression. Its input includes the task context, the
 77 parent formula, an annotated AST representation, fitted parameter values, summaries of already
 78 generated AST-rule mutations, extracted domain knowledge, and top-ranked historical expressions
 79 by training NMSE. This information allows the LLM to avoid duplicating existing programmatic
 80 mutations while proposing non-template local refinements informed by task context and domain
 81 knowledge.

82 The LLM Mutator uses two edit categories. ADD preserves the full parent and attaches out-of-
 83 library or domain-semantic material as a term, factor, or outer wrap. SUBST uses the annotated
 84 AST to replace a structurally mismatched subtree, so the full parent need not be preserved. In our
 85 implementation, the LLM proposes 20 candidates per parent with no fixed category quota; the prompt
 86 asks it to choose the mix according to the parent structure and fitted behavior.

Table C5: Categories of LLM-guided mutations.

Category	Description
ADD	Preserve f and attach non-template or domain-semantic content as $f + g$, $f \cdot g$, or $\phi(f)$.
SUBST	Replace a structurally wrong AST subtree with a different expression; the replaced subtree is not preserved.

87 **Degeneracy and overfitting screening** After constant fitting, each evaluated candidate is screened
 88 before it can re-enter the active search frontier. The screening is intentionally coefficient-aware: it uses
 89 the fitted constants rather than only the symbolic skeleton. Large-coefficient overfitting is checked
 90 only for sufficiently deep expressions, because shallow expressions often require large physical scale
 91 factors. Specifically, if the SymPy AST depth of the candidate is at least `overfit_min_depth`, any
 92 fitted coefficient with magnitude above 10^3 marks the node as OVERFIT. Independently of depth, the
 93 Mutator applies the simplification rules described after Algorithm 1, including small-coefficient term
 94 collapse, rational snapping of exponent parameters, elementary identities such as $\exp(0)$ and $\log(1)$,
 95 sinusoidal degeneracies, and merging of like terms.

96 The result is not only diagnostic. A node flagged as OVERFIT is excluded from all future parent-
 97 selection prompts. A node flagged as SIMPLIFIED is also excluded in its original form, while the
 98 simplified expression is treated as a new candidate and evaluated through the same optimizer and
 99 screening path. Thus the flag δ_g restricts search by preventing degenerate high-scoring expressions

100 from consuming Selector and mutation budget, while still preserving useful simplified descendants
 101 when the fitted constants reveal a simpler active formula.

102 **Configuration** Table C6 summarizes the Mutator configuration used in our symbolic-regression
 103 experiments. The deterministic channel is always enabled in the full FunctionEvolve setting, and the
 104 LLM channel is configured by the per-model YAML files in FunctionEvolve.

Table C6: Mutator configuration used in our experiments.

Parameter	Meaning	Value
mutation_channels	Candidate-generation channels in the full setting	AST deletion, AST addition, LLM mutation
llm_candidates_per_parent	Number of LLM proposals requested for each selected parent	20
mutator_seen_topk	Number of historical best expressions shown to the LLM Mutator	100
auto_mutation_summary	Maximum number of rule-generated mutation descriptions shown to the LLM	20
max_params	Maximum number of scalar parameters allowed in an evaluated candidate	10
overfit_min_depth	Minimum SymPy AST depth for degeneracy and overfitting screening	10
temperature	Sampling temperature for <i>Claude Opus 4.6</i> Mutator decoding	0.7
reasoning_effort	Reasoning setting for <i>GPT-5.2</i> Mutator decoding	medium
max_tokens	Maximum response length for Mutator decoding	128000

105 **Prompting interface** The prompt templates used by the LLM Mutator in the full FunctionEvolve
 106 setting are shown below. The system prompt defines the ADD/SUBST edit categories, domain-
 107 knowledge constraints, constant-notation convention, output schema, and allowed variables. The
 108 user prompt supplies the selected parent, its annotated AST, fitted parameter values, summaries
 109 of deterministic rule-generated candidates, and the current historical best formulas. This Mutator
 110 template is shared across LLM-SRBench and AI-Feynman; AI-Feynman changes the task background
 111 and the knowledge-section heading to dimension/variable-informed structures, but does not use a
 112 separate mutation prompt. The no-AST ablation uses the same JSON output contract but switches to
 113 a no-AST system prompt and removes the annotated AST block and AST-local substitution guidance
 114 from the user prompt.

```

LLM Mutator system prompt

You are a symbolic-regression expert. Propose {target_num} diverse
→ structural edits to the parent formula so that each resulting
→ candidate may fit the data better. Every edit takes the parent expression
→ and transforms it into one new candidate expression.

Structural Prior
Do NOT assume the ground-truth formula is a sum of terms. It may be a
→ compact monomial / product / ratio / composition, or a sum of several
→ mechanistic terms. Let the parent's current fit guide you: if the parent
→ already captures the trend, prefer small local refinements; if the parent
→ looks structurally wrong, prefer a rewrite. Do not blindly keep
→ growing the formula additively.

Two Kinds of Edit

```

The deterministic engine already covers simple template grafts (linear /
 ↪ power / exp / log / sin terms and factors, rational fractions, safe
 ↪ saturating divides, and single wraps) and all prunes / deletions /
 ↪ simplifications. See "Auto-Generated Candidates (do not repeat)" in the
 ↪ task. Your job is the part it cannot template:

- ****ADDITION**** (keep all of `f`; attach new material): `f + g`, `f * g`, or
 ↪ wrap `f` inside an outer function. Propose ****out-of-library /**
 ↪ **domain-semantic**** content, such as Arrhenius terms, Lorentz factors,
 ↪ cross-variable couplings, or nested compositions. The whole parent is
 ↪ preserved.
- ****SUBSTITUTION**** (discard a subtree, replace it): use the annotated AST to
 ↪ locate a structurally wrong subtree and replace it with a different
 ↪ structure (`t -> s`, where `t` no longer appears). Use this when the
 ↪ parent's shape is mismatched, not when you merely want to add a
 ↪ correction.

Do ****not**** propose pure simplifications / deletions -- the program handles
 ↪ those. Weight your {target_num} proposals toward whichever kind the
 ↪ parent's fit and structure call for; there is no fixed quota.

Elementary building blocks: power `x**c`, trigonometric `sin`/`cos`,
 ↪ exponential `exp`, logarithmic `log(1+x)`, and `sqrt`.

Non-Elementary Function Usage
 In addition to the elementary functions above, the following non-elementary
 ↪ functions are very common in scientific modeling and may be used as
 ↪ appropriate in either edit category:

- ****Abs(x)**** (absolute value): suitable for modulus operations in physical
 ↪ systems, amplitude extraction of sign-alternating variables in
 ↪ oscillatory systems. E.g. Abs(sin(x)) extracts oscillation amplitude,
 ↪ Abs(x)**c constructs V-shaped power law, log(1 + Abs(x)) symmetrizes
 ↪ logarithmic growth. Prefer Abs when a variable can be positive or
 ↪ negative but only the magnitude matters physically.
- ****Max(x, 0)**** (positive part / ReLU): suitable for describing piecewise
 ↪ behavior such as threshold activation, one-sided response. E.g. Max(x -
 ↪ c, 0) means response only above threshold c, Max(f(x), 0) truncates the
 ↪ negative part. Suitable for systems with critical points / activation
 ↪ thresholds.

- Syntax: use `Abs(x)` and `Max(x, 0)` in SymPy.

Using Domain Knowledge
 Design structures informed by the knowledge below. You may introduce a
 ↪ structure through either kind of edit: as an ****ADDITION**** (a new factor /
 ↪ term / wrap that preserves `f`) or as a ****SUBSTITUTION**** (rewrite a
 ↪ mismatched subtree). When an edit is motivated by this knowledge, state
 ↪ the basis in the `mutation` field.
 {domain_knowledge}

Constant Notation Convention
 Constant parameters should always appear in ****multiplicative form****, never
 ↪ alone in a denominator:

- Correct: `c0 * x`, `c0 * sin(c1 * x)`, `c0 / (x + c1)`
- Incorrect: `x / c0`, `sin(x / c0)` -- a constant in the denominator is
 ↪ numerically unstable. To express a "scaled variable", write `c * var`,
 ↪ not `var / c`.

Parameter Naming
 Any ****newly introduced**** constant must use a ****fresh**** `cK` that does not
 ↪ appear in the parent formula or its fitted parameters; keep the names of
 ↪ parent constants you retain.

Task Background
 {context}

```

## Output Format (strict compliance required)
Return only a JSON array of exactly {target_num} items.

Example item format:
[{"expression": "<SymPy-parseable formula>", "params": ["c0", "c1"],
  ↪ "mutation": "ADD: <what changed and why>"}]

- expression: use c0, c1, c2... for constants to be optimized; variables must
  ↪ come from the available variable list.
- params: list all parameter placeholders; if no constants, use [].
- mutation: must start with `ADD:` or `SUBST:`, followed by a brief
  ↪ rationale. When the edit is knowledge-driven, name the formula / law /
  ↪ structure it references.
- All functions must use SymPy/Python syntax: exp(x), log(x), sqrt(x),
  ↪ sin(x), cos(x), Abs(x), Max(x, 0).

## Available Variables
{variables}

```

LLM Mutator user prompt

```

## Parent Formula
{parent_formula}

## AST Structure
{labeled_ast}

## Fitted Parameters
{parent_fitted_params}

## Auto-Generated Candidates (do not repeat)
{auto_mutations_summary}

## Historical Best Formulas (top {topk})
{top_exprs}

Following the system instructions, propose {target_num} edits of two kinds:
  ↪ ADDITION (out-of-library / domain-semantic terms, factors, or wraps
  ↪ that preserve the parent) and SUBSTITUTION (rewrite a structurally
  ↪ wrong subtree located via the AST). Do not repeat the auto-generated
  ↪ template candidates above, and do not propose pure simplifications. There
  ↪ is no fixed quota -- weight the mix toward what the parent's AST and
  ↪ current fit suggest.

```

115 **Degenerated Mutator** For ablations, FunctionEvolve supports three degenerated Mutator variants.
 116 The first variant disables the LLM mutation channel and keeps only programmatic AST-rule mutations,
 117 namely rule deletion and template-based rule addition. The second variant disables the programmatic
 118 rule channel and keeps only LLM-generated ADD/SUBST edits, while still providing the LLM
 119 with the standard parent-level structural context. The third variant also uses only LLM-generated
 120 ADD/SUBST edits, but further removes the annotated AST representation and replaces AST-local
 121 mutation guidance with parent-formula subexpression guidance in the LLM prompt. The second and
 122 third variants do not carry a hidden blanket preprocessing stage. This set of variants separates the
 123 effects of deterministic AST-rule expansion, LLM-guided local structural refinement, and explicit
 124 AST visibility in the mutation interface.

125 C6 Optimizer

126 For each candidate expression, the structure-aware coefficient optimizer fits scalar coefficients under
 127 a fixed symbolic skeleton and returns the numerical score used by the evolutionary search. Since
 128 inaccurate coefficient fitting can make a correct skeleton appear unpromising, this appendix details

129 how FunctionEvolve uses expression structure during coefficient fitting, following the same sequence
 130 as the main text.

131 **Expression analysis before optimization** Before numerical search, the optimizer parses the
 132 candidate into a symbolic expression and extracts parameter-specific constraints from the expression
 133 structure. Parameters that appear as exponents over feature-dependent bases are treated carefully,
 134 especially when the base can be negative, because arbitrary real exponents can leave the real domain.
 135 In this case the implementation evaluates such powers through a real-valued safe-power wrapper
 136 and snaps the exponent to the nearest multiple of $1/3$ when needed. The optimizer also identifies
 137 parameters that should be positive or searched over a smaller range, such as coefficients inside
 138 logarithms, exponentials, trigonometric arguments, or power exponents. The default full-parameter
 139 box is $[-100, 100]$; rational-sensitive exponents use $[-10, 10]$, positive parameters use $[10^{-6}, 100]$,
 140 small parameters use $[-5, 5]$, and parameters that are both positive and small use $[10^{-6}, 5]$. In
 141 addition, data-dependent bounds are computed for parameters controlling exponential growth and
 142 feature offsets. For terms of the form $\exp(c_i g(\mathbf{x}))$, the coefficient bound is chosen so that the absolute
 143 exponential argument is at most 10 over the training data. For offset parameters in $\exp(g(x - c_i))$ or
 144 $(x - c_i)^p$, the search interval is the observed feature range enlarged by $\max(0.2 \text{ range}(x), 10)$.

145 **Variable projection** The main optimization path first attempts to separate linear and nonlinear
 146 parameters. Many candidates can be written as

$$f(\mathbf{x}; \mathbf{c}) = f(\mathbf{x}; \mathbf{c}_L, \mathbf{c}_N) = \psi(\mathbf{x}; \mathbf{c}_N) + \sum_{j=1}^m c_{L,j} \phi_j(\mathbf{x}; \mathbf{c}_N),$$

147 where \mathbf{c}_L are linear coefficients and \mathbf{c}_N are nonlinear parameters. For any fixed \mathbf{c}_N , the optimal
 148 \mathbf{c}_L is obtained by ordinary least squares, so the explicit search only needs to explore the nonlinear
 149 subspace:

$$\min_{\mathbf{c}_N} \min_{\mathbf{c}_L} \left\| \mathbf{y} - \psi(\mathbf{X}; \mathbf{c}_N) - \sum_{j=1}^m c_{L,j} \phi_j(\mathbf{X}; \mathbf{c}_N) \right\|_2^2.$$

150 In practice, the optimizer differentiates the expression with respect to candidate parameters, selects a
 151 maximal subset that is jointly affine, and constructs the OLS basis functions from the corresponding
 152 partial derivatives after setting the linear parameters to zero. The remaining fixed part ψ is sub-
 153 tracted from the target before solving the linear coefficients analytically at each nonlinear parameter
 154 assignment.

155 **Structured pre-search for difficult nonlinear parameters** Some nonlinear parameters are particu-
 156 larly difficult for continuous optimization. For compound power structures such as $(x + c_1)^{c_2}$,
 157 where the power exponent is itself a single parameter and the base contains another parameter, the
 158 optimizer first enumerates

$$\{1, 2, 1/2, 3, 1/3, -1, 3/2, 4, 5, -1/2, -2, -3\}$$

159 for the exponent and runs variable projection on the remaining parameters under each fixed value.
 160 This pre-search is executed before the main variable-projection stage and can consume up to 70%
 161 of the variable-projection time budget. Inside variable projection, any remaining power-exponent
 162 parameters are handled by a second candidate grid,

$$\{1/3, 1/2, 1, 3/2, 2, 3, 4, 5, -1/3, -1/2, -1, -2, -3\},$$

163 using a sequential greedy strategy when multiple exponents are present. For each fixed exponent
 164 value, the remaining nonlinear parameters are searched by trust-region least squares with five random
 165 restarts, and linear coefficients are still solved by OLS. For center or offset parameters appearing
 166 in Gaussian-like, exponential-shift, or shifted-power forms, the optimizer detects $(x - c_i)$ -style
 167 subexpressions and scans 100 equally spaced candidate centers between the observed minimum
 168 and maximum of the corresponding feature. These structured pre-search steps provide strong initial
 169 basins before the general nonlinear search begins.

170 **Global search over nonlinear parameters** After variable projection, the remaining objective over
171 \mathbf{c}_N is lower-dimensional but can still be highly non-convex. FunctionEvolve therefore searches
172 the nonlinear subspace with trust-region least squares, CMA-ES, and differential evolution, each
173 using an independent initialization drawn from the same constraint-aware sampler. The variable-
174 projection path uses the first 45% of the optimizer timeout, with the remaining time in that window
175 divided approximately equally across these three continuous search stages after structured pre-search.
176 This design focuses global exploration on the parameters that determine the nonlinear shape of the
177 expression, while avoiding unnecessary search over linear coefficients that can be solved exactly by
178 OLS.

179 The fallback condition is explicit in the implementation. Let $\sigma_y^2 = \text{Var}(\mathbf{y}_{\text{train}})$, with a unit fallback
180 for nearly constant targets, and define the early-success threshold $\tau = 10^{-10}\sigma_y^2$. Variable projection is
181 treated as unavailable when no valid decomposition is produced, for example because the expression
182 has no jointly affine coefficient, no basis functions can be constructed, or OLS/basis/fixed-part
183 evaluation becomes non-finite. It is treated as insufficient when the best MSE found so far remains
184 above τ . In either case, the optimizer falls back to full-parameter numerical search until 90% of the
185 total timeout, allocating the remaining fallback budget equally to full-parameter trust-region least
186 squares, CMA-ES, and differential evolution. Thus “insufficient” is not a hidden symbolic criterion;
187 it is the same MSE threshold used for early termination of the optimizer.

188 **Local refinement** The best solutions obtained from the preceding stages are then refined with
189 gradient-based local optimization, implemented as L-BFGS-B over the same parameter bounds.
190 This polishing stage uses the final 10% of the total timeout. If parent parameters are available from
191 the evolutionary tree, the optimizer also performs an additional warm-started L-BFGS-B pass after
192 copying the overlapping parent parameter prefix into the current skeleton.

193 **Snap and refit** Finally, the optimizer performs optional snapping for exponent-like or rational-
194 sensitive parameters. Parameters that must remain stable over negative bases are snapped to nearby
195 rational values whose reduced denominators are odd. Power exponents are then tested against the
196 same nearby integer/rational grid used above, restricted to candidates within distance 3 of the current
197 value. Crucially, snapping is followed by an L-BFGS-B refit with the snapped exponent fixed; the
198 snapped form is accepted only if the refit preserves or improves the numerical objective. This makes
199 the final expression more stable and interpretable without sacrificing the fitness estimate used by the
200 search.

201 C7 Optimizer Benchmark Variants

202 The optimizer benchmark in Section 4.5 is built from ground-truth LLM-SRBench skeletons so
203 that failure can be attributed to coefficient fitting rather than structural search. Numeric constants
204 are replaced by symbolic parameters, parameter couplings are decoupled when possible, and the
205 resulting exact skeleton forms the original-expression group. We then create controlled variants that
206 preserve the same target function under a known parameter assignment. The composite zero-term
207 variants add zero-amplitude nonlinear terms, either $c_a \sin(\log(1 + c_b x) + c_c)$ or $c_a \exp(c_b \cos(c_c x))$
208 with $c_a = 0$, testing whether an optimizer can ignore unnecessary nonlinear additive structure. The
209 power-augmentation variants introduce identity power transformations by replacing a feature with
210 x^{c_a} or raising the whole expression to c_a , with $c_a = 1$, testing difficult exponent-like parameters. The
211 rational zero-term variants add terms of the form $(c_a x + c_b)/(c_c x + c_d)$, or the analogous numerator
212 using a second feature, with $c_a = c_b = 0$ and $c_c = c_d = 1$. These four groups are the categories
213 reported in Figure 7.

214 D Additional Experimental Results

215 D1 Complexity-aware Final Selection Details

216 The complexity-aware selectors in Section 4.7 are applied only after the evolutionary search has
217 finished. They do not choose parents, generate mutations, fit coefficients, or alter the trajectory. For
218 each task, we collect the full candidate trajectory, preserve the training-NMSE ranking used by the
219 search, and compute simple structural features for each expression. The selectors then choose a fixed

220 reporting shortlist from this already generated pool. Test and OOD NMSE are never used by these
 221 selectors.

222 Let candidate i have training error e_i , original training-NMSE rank r_i , and structural features: tree
 223 size s_i , operator count o_i , fitted-parameter count p_i , and special-function count h_i . We use a weighted
 224 complexity score

$$q_i = s_i + w_o o_i + w_p p_i + w_h h_i,$$

225 where the weights are fixed before evaluation. Pareto selection performs non-dominated sorting over
 226 $(\log e_i, q_i)$: a candidate is dominated if another candidate has no larger value in both objectives and
 227 a strictly smaller value in at least one. Candidates from the first front are selected first, ordered by
 228 $(\log e_i, q_i, r_i)$; if the shortlist is not full, the selected front is removed and the next front is added in
 229 the same way.

230 Occam selection first restricts the pool to candidates with near-best training fit. Specifically, if e_* is
 231 the best finite training NMSE, the near-best set contains candidates satisfying

$$\log_{10}(\max(e_i, 10^{-300})) - \log_{10}(\max(e_*, 10^{-300})) \leq \Delta.$$

232 Within this near-best set, candidates are ranked by $(q_i, \log e_i, r_i)$, so simpler expressions are preferred
 233 only after the training error is already close to the best observed fit. If the near-best set is too small to
 234 fill the shortlist, the rule falls back to the full pool with the same complexity-first ordering.

235 MDL selection uses a single scalar objective,

$$m_i = \log e_i + \alpha p_i + \beta s_i + \beta_o o_i,$$

236 and returns the candidates with the smallest m_i , with the original rank r_i used only as a deterministic
 237 tie-breaker. This rule approximates a description-length tradeoff: the log training loss rewards fit,
 238 while parameter, tree-size, and operator penalties discourage unnecessarily complex formulas. All
 239 three selectors therefore test whether post-hoc complexity-aware reporting can recover exact symbolic
 240 forms that were generated by the search but ranked below numerically strong surrogate expressions
 241 by training NMSE alone.

242 D2 Non-MatSci Failure Correlation Audit

243 Table D1 reports the pairwise linear-dependence audit for the twelve FunctionEvolve failure cases
 244 (tasks with SA@50 = 0) outside the MatSci subset. Unlike MatSci, these domains do not exhibit
 245 a dataset-wide input collapse, but several individual failures still contain highly correlated variable
 246 pairs. Four of these tasks—CRK0, CRK6, CRK22, and PO17—do eventually recover a symbolically
 247 correct expression, but only among candidates ranked beyond the top-50 budget (at ranks 693, 229,
 248 313, and 224, respectively); they therefore count as SA@50 failures here even though they are not
 249 failures under the full-trajectory exact-match audit.

Table D1: Pairwise linear dependence in non-MatSci failures.

Case	Variable pair	R^2
BPG4	t, P	0.723803
BPG20	t, P	0.674447
CRK0	t, A	0.208901
CRK6	t, A	0.951128
CRK22	t, A	0.517110
250 CRK28	t, A	0.999234
CRK29	t, A	0.732757
PO0	x, t	0.001431
PO16	x, t	0.004350
PO17	x, v	0.028476
PO23	x, v	0.964941
PO43	x, v	0.368555

251 D3 Baseline NMSE Summary

252 Table D2 reports the selected non-FunctionEvolve baselines from the same CSV. Here symbolic
 253 accuracy is reported as SA@50 (SA@1), Train/Test/OOD NMSE are split-wise medians over 129
 254 tasks, and Test Acc $_{\tau}$ counts tasks with test maximum relative error at most τ .

255 The corresponding per-task records are available in the GitHub raw data files described above.

Table D2: Baseline NMSE summary for methods run with *Claude Opus 4.6*. Symbolic accuracy is reported as SA@50 (SA@1). NMSE entries are medians over 129 tasks, and accuracy entries are raw test-set task counts.

Method	SA@50 (@1) ↑	Train NMSE ↓	Test NMSE ↓	OOD NMSE ↓	Test Acc _{0.1} ↑	Test Acc _{0.01} ↑	Test Acc _{0.001} ↑
Direct Prompting	2 (1)	1.24e-3	1.36e-3	7.62e-2	18	7	4
OpenEvolve [Sharma, 2025]	24 (5)	4.50e-6	4.30e-6	6.52e-3	27	8	1
LLM-SR [Shojaee et al., 2024]	24 (11)	2.62e-6	9.80e-7	4.45e-4	40	13	5

Table D3: Extended ablation results on 129 LLM-SRBench tasks. Entries report SA@50 (SA@1).

Method	Model	Chemistry (36)	Biology (24)	Physics (44)	Materials Science (25)	Total (129)
Full	<i>GPT-5.2-medium</i>	30 (13)	20 (15)	37 (36)	16 (5)	103 (69)
w/o All	<i>GPT-5.2-medium</i>	12 (4)	18 (1)	2 (1)	3 (0)	35 (6)
w/o Generator	<i>GPT-5.2-medium</i>	21 (9)	20 (13)	29 (24)	9 (3)	79 (49)
w/o Selector	<i>GPT-5.2-medium</i>	20 (13)	17 (12)	14 (12)	11 (7)	62 (44)
w/o LLM Mutator	<i>GPT-5.2-medium</i>	12 (7)	14 (11)	12 (8)	7 (1)	45 (27)
w/o AST Mutator	<i>GPT-5.2-medium</i>	27 (12)	18 (14)	14 (13)	11 (3)	70 (42)
w/o Structure-aware Optimizer	<i>GPT-5.2-medium</i>	18 (3)	14 (7)	12 (5)	2 (1)	46 (16)
Full	<i>Claude Opus 4.6</i>	31 (16)	22 (16)	39 (34)	15 (6)	107 (72)
w/o All	<i>Claude Opus 4.6</i>	12 (4)	16 (5)	4 (1)	2 (0)	34 (10)
w/o Generator	<i>Claude Opus 4.6</i>	27 (12)	22 (14)	33 (29)	9 (3)	91 (58)
w/o Selector	<i>Claude Opus 4.6</i>	25 (13)	20 (11)	20 (18)	9 (4)	74 (46)
w/o LLM Mutator	<i>Claude Opus 4.6</i>	11 (8)	15 (11)	13 (10)	7 (2)	46 (31)
w/o AST Mutator	<i>Claude Opus 4.6</i>	30 (16)	22 (11)	23 (20)	9 (3)	84 (50)
w/o AST Structure	<i>Claude Opus 4.6</i>	24 (14)	20 (15)	8 (7)	8 (4)	60 (40)
w/o Structure-aware Optimizer	<i>Claude Opus 4.6</i>	17 (6)	17 (4)	16 (12)	3 (0)	53 (22)

256 D4 Complete Ablation Results

257 Table D3 reports the domain-wise symbolic-accuracy ablation results for both *GPT-5.2-medium* and
 258 *Claude Opus 4.6*. Each entry gives SA@50 (SA@1). Tables D4 and D5 complement this view with
 259 aggregate NMSE and numerical-accuracy summaries for the same ablation settings. The two model
 260 backbones show the same qualitative pattern: removing the LLM Mutator or replacing the structure-
 261 aware coefficient optimizer with L-BFGS produces the largest SA@50 drops, while removing the
 262 Generator, Selector, or AST Mutator also consistently reduces symbolic recovery.

263 **NMSE and numerical accuracy summaries** The following tables are computed from the NMSE
 264 result records and report all ablation settings used in our experiments. The records contain five
 265 aggregate rows per run (BPG_all, CRK_all, MatSci_all, P0_all, and Total_all); these tables
 266 use only the 129 individual benchmark tasks. In each table, *Method* names the same setting used in
 267 the ablation study, *SA* is the number of exact symbolic matches, Train/Test/OOD NMSE report the
 268 median normalized mean squared error on the corresponding split, and Test Acc_τ reports the number
 269 of tasks with test maximum relative error at most τ. To keep the appendix compact, we omit the full
 270 per-task detail tables; detailed raw data are available at [https://anonymous.4open.science/r/](https://anonymous.4open.science/r/FunctionEvolve)
 271 *FunctionEvolve*.

272 ***GPT-5.2-medium*** Table D4 reports the *GPT-5.2-medium* backbone. The *w/o Generator*, *w/o*
 273 *Selector*, *w/o LLM Mutator*, *w/o AST Mutator*, *w/o Structure-aware Optimizer*, and *w/o All* rows
 274 follow the ablation definitions in Section 4.3: they respectively remove LLM-based initialization,
 275 LLM-based parent selection, LLM mutation proposals, AST-rule mutations, the structure-aware
 276 coefficient optimizer, and the combined Generator/Selector/AST-Mutator/Structure-aware-Optimizer
 277 stack.

Table D4: Complete ablation NMSE summary for *GPT-5.2-medium*. NMSE entries are medians over 129 tasks, and accuracy entries are raw test-set task counts.

278

Method	SA \uparrow	Train NMSE \downarrow	Test NMSE \downarrow	OOD NMSE \downarrow	Test Acc _{0.1} \uparrow	Test Acc _{0.01} \uparrow	Test Acc _{0.001} \uparrow
Full	103	1.82e-13	2.08e-13	2.21e-10	111	88	73
w/o All	35	4.20e-7	4.27e-7	3.98e-4	49	19	11
w/o Generator	79	2.88e-13	2.42e-13	2.38e-9	107	81	71
w/o Selector	62	3.77e-13	4.63e-13	3.72e-9	99	72	63
w/o LLM Mutator	45	1.24e-12	1.16e-12	1.13e-8	91	67	55
w/o AST Mutator	70	3.77e-13	3.47e-13	4.14e-9	99	74	66
w/o Structure-aware Optimizer	46	4.01e-8	4.33e-8	1.80e-5	69	42	22

280 The corresponding per-task records are available in the GitHub raw data files described above.

281 **Claude Opus 4.6** Table D5 uses the same column definitions for the *Claude Opus 4.6* backbone. In
 282 addition to the main ablation rows, *w/o AST in LLM Interfaces* keeps the LLM channels but removes
 283 AST-heavy information from their prompts, and *Rule-only + Structure-aware Optimizer* disables
 284 the Generator, the LLM Selector, and the LLM Mutator while retaining the default structure-aware
 285 coefficient optimizer.

Table D5: Complete ablation NMSE summary for *Claude Opus 4.6*. NMSE entries are medians over 129 tasks, and accuracy entries are raw test-set task counts.

286

Method	SA \uparrow	Train NMSE \downarrow	Test NMSE \downarrow	OOD NMSE \downarrow	Test Acc _{0.1} \uparrow	Test Acc _{0.01} \uparrow	Test Acc _{0.001} \uparrow
Full	107	1.34e-13	1.38e-13	1.78e-10	113	94	78
w/o All	34	2.31e-7	1.93e-7	2.15e-4	53	27	15
w/o Generator	91	2.43e-13	2.06e-13	4.23e-10	110	87	75
w/o Selector	74	4.14e-13	4.65e-13	4.71e-9	100	78	63
w/o LLM Mutator	46	1.04e-12	1.01e-12	1.09e-8	89	67	55
w/o AST Mutator	84	2.43e-13	2.06e-13	2.52e-9	108	83	71
w/o AST Structure	60	4.25e-13	5.09e-13	6.73e-9	96	71	59
w/o Structure-aware Optimizer	53	5.37e-9	8.19e-9	5.68e-6	66	43	27
Rule-only + Structure-aware Optimizer	29	1.42e-10	1.47e-10	3.65e-7	78	53	39

288 The corresponding per-task records are available in the GitHub raw data files described above.

289 D5 Numerical Accuracy at Stricter Tolerances

290 We distinguish two tolerance-based task-count metrics. Our Acc_τ follows the convention used in
 291 LLM-SRBench reporting and in the main text: a task is counted only when the top-1 prediction has
 292 relative error at most τ at every evaluation point, equivalently when its maximum relative error is at
 293 most τ . For a single test task, this indicator can be written as

$$\text{Acc}_\tau = \mathbf{1} \left(\max_{1 \leq i \leq N_{\text{test}}} \left| \frac{\hat{y}_i - y_i}{y_i} \right| \leq \tau \right).$$

294 A relaxed variant, denoted $95\% \text{Acc}_\tau$, counts a task when at least 95% of its evaluation points have
 295 relative error at most τ .

296 SR-Scientist [Xia et al., 2025] reports this relaxed $95\% \text{Acc}_\tau$ metric for $\tau = 0.01$ and $\tau = 0.001$,
 297 which is not directly aligned with the reporting convention in LLM-SRBench-style papers or with
 298 our main-text Acc_τ numbers. Table D6 therefore reports test-set entries as Acc_τ ($95\% \text{Acc}_\tau$): values
 299 cited from SR-Scientist appear only in parentheses, while results from our executable runs report
 300 strict all-point counts with the corresponding relaxed 95% counts in parentheses. Table D7 uses the
 301 same convention for OOD results.

302 D6 Reliability Audit for LLM-as-a-Judge Symbolic Accuracy

303 Symbolic accuracy at k counts a task as successful if any of the top- k candidates is mathematically
 304 equivalent to the ground-truth expression. In this equivalence check, ground-truth constants are fixed,
 305 candidate constants are free, and physics-oscillator (PO) variables are allowed to take negative values,
 306 so expressions such as $v**c$ are not treated as equivalent to $\text{Abs}(v)**c$. To reduce dependence on
 307 a single model judgment, each verification case is judged independently by *GPT-5.2* and *Claude*
 308 *Opus 4.6*. If their valid verdicts disagree, or if either run returns `verify_error`, the case is manually
 309 adjudicated.

310 We audit 500 verification cases sampled randomly. For *Opus 4.6*, repeated rows caused by retries are
 311 deduplicated by `sample_id`; when available, the final non-`verify_error` result is used. Table D8

Table D6: Test-set numerical accuracy at stricter tolerances on the 129-task synthetic subset of LLM-SRBench. Entries report raw task counts as Acc_τ ($95\%Acc_\tau$), with $\tau = 0.01$ or 0.001 ; parenthesized-only entries are the relaxed $95\%Acc_\tau$ results cited from Xia et al. [2025]. Best all-point Acc_τ values are shown in bold, while the ground-truth row is a reference row. Entries marked with * are converted from percentages reported in Xia et al. [2025] using the corresponding domain sizes, with counts rounded independently.

Model	Chemistry (36)		Biology (24)		Physics (44)		Materials Science (25)		Total (129)	
	$Acc_{0.01} \uparrow$	$Acc_{0.001} \uparrow$	$Acc_{0.01} \uparrow$	$Acc_{0.001} \uparrow$	$Acc_{0.01} \uparrow$	$Acc_{0.001} \uparrow$	$Acc_{0.01} \uparrow$	$Acc_{0.001} \uparrow$	$Acc_{0.01} \uparrow$	$Acc_{0.001} \uparrow$
<i>Direct Prompting</i>										
<i>Claude Opus 4.6</i>	0 (1)	0 (0)	2 (4)	1 (2)	2 (3)	2 (2)	3 (10)	1 (5)	7 (18)	4 (9)
<i>OpenEvolve [Sharma, 2025]</i>										
<i>Claude Opus 4.6</i>	5 (8)	0 (2)	1 (2)	0 (0)	0 (9)	0 (2)	2 (11)	1 (1)	8 (30)	1 (5)
<i>LLM-SR [Shojaee et al., 2024]</i>										
<i>Claude Opus 4.6</i>	5 (9)	1 (1)	1 (6)	1 (1)	0 (7)	0 (2)	7 (19)	3 (10)	13 (41)	5 (14)
<i>SR-Scientist [Xia et al., 2025]</i>										
<i>Qwen3-Coder-480B-A35B-Instruct*</i>	(15)	(2)	(12)	(6)	(15)	(6)	(22)	(17)	(63)	(32)
<i>GLM-4.5-Air*</i>	(16)	(4)	(10)	(4)	(16)	(7)	(20)	(18)	(62)	(32)
<i>GPT-OSS-120B*</i>	(29)	(23)	(16)	(10)	(18)	(15)	(19)	(15)	(82)	(64)
<i>GPT-OSS-20B*</i>	(18)	(8)	(8)	(5)	(13)	(7)	(16)	(10)	(55)	(30)
<i>Qwen3-Coder-30B-A3B-Instruct*</i>	(8)	(2)	(5)	(2)	(8)	(4)	(20)	(13)	(42)	(21)
<i>Qwen3-Coder-30B-A3B-Instruct + RL*</i>	(13)	(3)	(7)	(3)	(11)	(5)	(21)	(16)	(53)	(27)
<i>FunctionEvolve (Ours)</i>										
<i>GPT-5.2-medium</i>	26 (33)	22 (32)	14 (23)	9 (23)	28 (36)	24 (32)	20 (25)	18 (24)	88 (117)	73 (111)
<i>Claude Opus 4.6</i>	27 (35)	23 (34)	15 (23)	9 (23)	31 (34)	27 (34)	21 (25)	19 (22)	94 (117)	78 (113)
<i>Reference: GT equations</i>	27 (35)	24 (35)	14 (23)	10 (23)	36 (39)	33 (39)	25 (25)	25 (25)	102 (122)	92 (122)

Table D7: OOD numerical accuracy at stricter tolerances on the 129-task synthetic subset of LLM-SRBench. Entries report raw task counts as Acc_τ ($95\%Acc_\tau$), with $\tau = 0.01$ or 0.001 ; best all-point Acc_τ values are shown in bold.

Model	Chemistry (36)		Biology (24)		Physics (44)		Materials Science (25)		Total (129)	
	$Acc_{0.01} \uparrow$	$Acc_{0.001} \uparrow$	$Acc_{0.01} \uparrow$	$Acc_{0.001} \uparrow$	$Acc_{0.01} \uparrow$	$Acc_{0.001} \uparrow$	$Acc_{0.01} \uparrow$	$Acc_{0.001} \uparrow$	$Acc_{0.01} \uparrow$	$Acc_{0.001} \uparrow$
<i>Direct Prompting</i>										
<i>Claude Opus 4.6</i>	2 (2)	0 (1)	3 (4)	1 (2)	3 (3)	2 (2)	13 (13)	11 (11)	21 (22)	14 (16)
<i>OpenEvolve [Sharma, 2025]</i>										
<i>Claude Opus 4.6</i>	6 (7)	1 (1)	3 (3)	1 (2)	2 (9)	0 (2)	19 (21)	14 (14)	30 (40)	16 (19)
<i>LLM-SR [Shojaee et al., 2024]</i>										
<i>Claude Opus 4.6</i>	7 (8)	2 (2)	4 (6)	1 (2)	2 (7)	0 (2)	20 (20)	17 (17)	33 (41)	20 (23)
<i>FunctionEvolve (Ours)</i>										
<i>GPT-5.2-medium</i>	31 (34)	26 (31)	16 (23)	10 (20)	29 (35)	21 (30)	25 (25)	25 (25)	101 (117)	82 (106)
<i>Claude Opus 4.6</i>	32 (35)	29 (34)	16 (23)	10 (21)	32 (34)	24 (33)	25 (25)	25 (25)	105 (117)	88 (113)

312 summarizes agreement. The judges agree on 476 valid match/no_match decisions. There are 21
313 valid verdict disagreements and three cases involving `verify_error`, so only 24/500 cases require
314 manual intervention. Table D9 reports the resulting judge accuracies after manual adjudication, with
315 and without counting the single unscorable case in the denominator.

Table D8: Reliability audit of the LLM-as-a-judge protocol for symbolic accuracy.

Category	Count	Rate
Total audited samples	500	100.0%
Same valid verdict	476	95.2%
Valid verdict disagreement	21	4.2%
Cases involving <code>verify_error</code>	3	0.6%
Manual intervention cases	24	4.8%

Table D9: Judge accuracy after manual adjudication. The single unscorable case had no extractable final candidate formulas.

Judge	Correct / 499	Accuracy / 499	Correct / 500	Strict accuracy / 500
<i>GPT-5.2</i>	482	96.59%	482	96.40%
<i>Claude Opus 4.6</i>	493	98.80%	493	98.60%

Table D10 lists the 24 cases requiring manual intervention. Among the 23 scorable cases in this set, *GPT-5.2* is correct on 6 and *Opus 4.6* is correct on 17. The only unscorable case is `sample_id=294`, where both judges fail because the log contains no extractable final candidate formulas.

Table D10: Manual adjudication for cases where the two judges disagreed or at least one returned `verify_error`.

ID	Case	<i>GPT-5.2</i>	<i>Opus 4.6</i>	Final	Main reason
002	BPG5	no_match	match	match	Rational common-denominator rewriting makes a candidate equivalent.
038	BPG1	no_match	match	match	Candidate has both $P \exp(ct)$ and a rational term that can match after rewriting.
044	BPG23	match	no_match	match	Candidate can represent the polynomial plus $P \exp(cP)$ structure.
080	PO20	no_match	match	no_match	PO domain requires <code>Abs(v); v**c*x</code> is not equivalent.
082	PO34	no_match	match	no_match	Same PO-domain absolute-value issue.
112	CRK1	match	no_match	match	Candidate can reduce to polynomial terms plus a phase-shifted log-trigonometric term.
145	MatSci1	match	no_match	no_match	Required Arrhenius term $\exp(-c/T)$ is absent.
169	CRK29	no_match	match	match	Denominator form can represent the rational term and the linear/exponential terms.
173	MatSci14	no_match	match	match	Candidate can represent the required linear-in- T and e^P cross terms.
231	CRK19	match	no_match	no_match	Requires $\sin(\log(A + 1))$; candidates have no-phase cosine or wrong log arguments.
257	CRK22	no_match	match	match	Common-denominator rewriting matches the ground truth.
294	MatSci12	verify_error	verify_error	unscorable	No final formulas or code snippets were extractable from the log.
304	BPG3	no_match	match	match	Candidate has the needed P^3 , P^2 , and $P \exp(cP)$ basis functions.
315	MatSci8	match	no_match	match	Candidate can represent $T\epsilon^P$, $T\epsilon$, ϵ^P , and ϵ .
362	CRK3	no_match	match	match	Candidate has $A \exp(ct)$, A^2 , and a phase-shifted $\sin(\log(A + 1))$ term.
363	MatSci2	verify_error	no_match	no_match	Candidates lack the required combination of ϵ^3 , $T \exp(-\epsilon)$, and $\exp(-\epsilon)$.
368	MatSci18	verify_error	match	match	Candidate has $\epsilon^2 + \epsilon(T + c)^2$.
371	PO12	no_match	match	no_match	<code>sqrt(v**c)</code> is not a valid substitute for <code>Abs(v)**(1/3)</code> on the PO domain.
374	CRK22	no_match	match	match	Common-denominator rewriting matches the ground truth.
383	MatSci28	no_match	match	match	Candidate contains the required $T\epsilon$, $T \log(\epsilon + 1)$, and ϵ^2 terms.
386	PO22	no_match	match	match	Candidate can express $\exp(- x)$ via $\exp(c/\sqrt{x-2})$.
391	BPG11	no_match	match	match	Candidate can represent P , P^2 , $P^{1/3}$, and $P \exp(ct)$.
415	BPG16	no_match	match	match	Candidate can reduce to $P^3 + P^2 + P^{1/3}$.
439	BPG1	no_match	match	match	Candidate can match with $P \exp(ct)$ plus a reciprocal rational term.

This audit does not assume that LLM judges are infallible. Instead, it shows that single-judge errors are measurable and rare under our prompt, and that the reported $SA@k$ values use a two-judge-plus-manual-adjudication protocol rather than unchecked single-model judgments. The main *GPT-5.2* error mode is rejecting valid rational-function equivalences that become clear after common-denominator rewriting. The main *Opus 4.6* error mode is over-relaxing domain constraints, especially treating `v**c` as if it could stand for `Abs(v)**c` in PO tasks where negative velocities are allowed.